SANDIA REPORT SAND85-8249 • Unlimited Release • UC-62a
Printed December 1985

Numerical Modeling of a Solid Particle Solar Central Receiver

G. H. Evans, W. G. Houf, R. Greif and C. Crowe

Prepared by
Sandia National Laboratories
Albuquerque, New Mexico 87185 and Livermore, California 94550
for the United States Department of Energy
under Contract DE-AC04-76DP00789

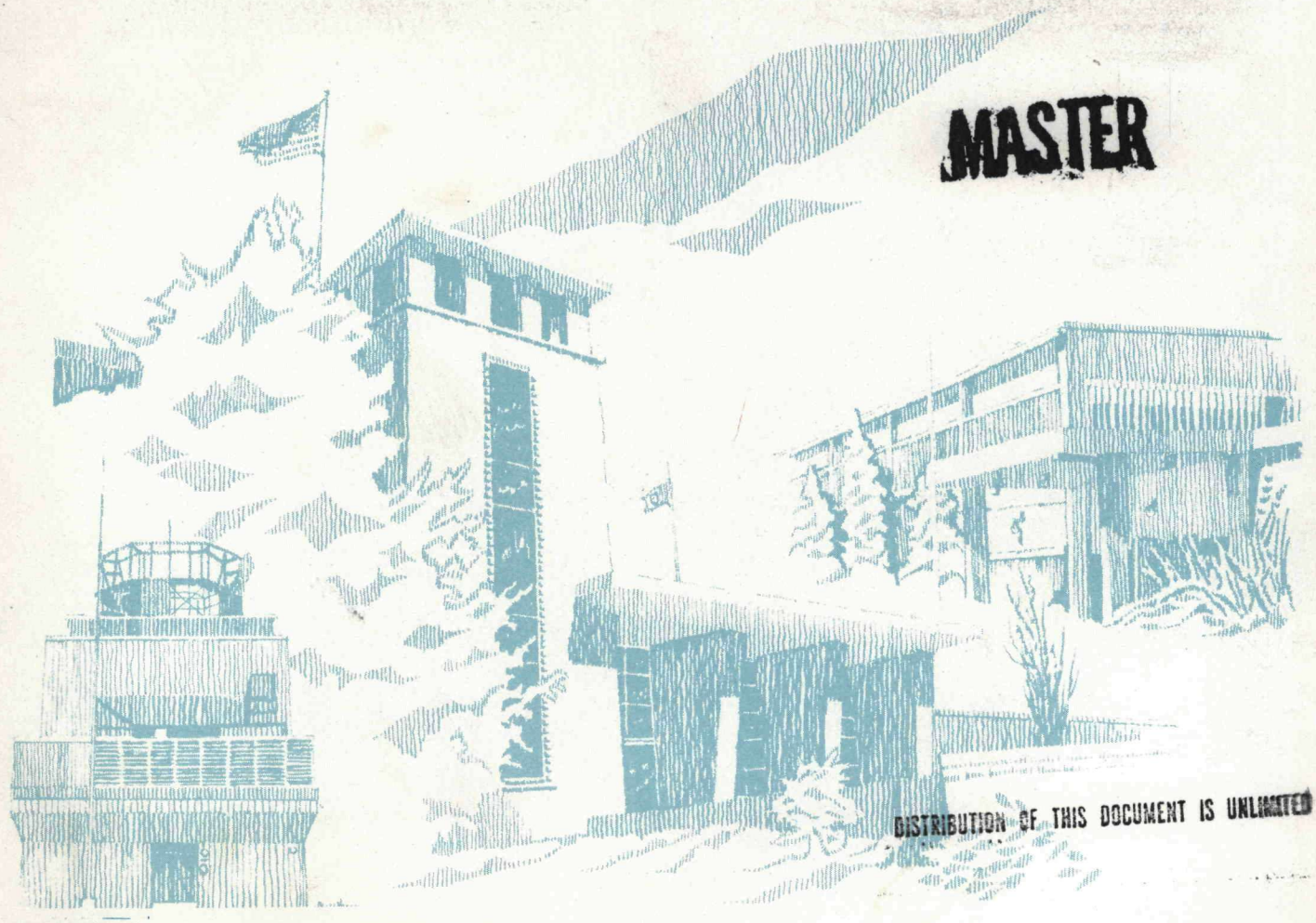

DO NOT MICROFILM
COVER

Issued by Sandia National Laboratories, operated for the United States Department of Energy by Sandia Corporation.

Printed in the United States of America
Available from
National Technical Information Service
5285 Port Royal Road
Springfield, VA 22161

NTIS price codes
Printed copy: **A04**
Microfiche copy: A01

DISCLAIMER

SAND--85-8249

DE86 005066

UC-62a

SAND85-8249
Unlimited Release
Printed December 1985

NUMERICAL MODELING OF A SOLID PARTICLE SOLAR CENTRAL RECEIVER

Gregory H. Evans and William G. Houf
Computational Mechanics Division
Sandia National Laboratories, Livermore

Ralph Greif
Mechanical Engineering Department
University of California
Berkeley, Ca. 94720

Clayton Crowe
Mechanical Engineering Department
Washington State University
Pullman, Wa. 99164

ABSTRACT

The flow of air and particles and the heat transfer inside a solar heated, open cavity containing a falling cloud of 100-1000 micron solid particles have been studied. Two-way momentum and thermal coupling between the particles and the air is included in the analysis along with the effects of radiative transport within the particle cloud, among the cavity surfaces, and between the cloud and the surfaces. The flow field is assumed to be two dimensional with steady mean quantities. The PSI-Cell (particle source in cell) computer code is used to describe the gas-particle interaction. The method of discrete ordinates is used to obtain the radiative transfer within the cloud.

The results include the velocity and temperature profiles of the particles and the air. In addition, the thermal performance of the solid particle solar receiver has been determined as a function of the following particle parameters: size, mass flow rate, absorptivity, and infrared scattering albedo. Other parameters which have been varied include the incident solar flux (both magnitude and distribution) and receiver size. A forced flow, applied across the cavity aperture, has also been investigated as a means of decreasing convective heat loss from the cavity.

Comparison of the results from the model has been made with an experiment performed at the radiant heat facility in Albuquerque. The model has also been used to predict the entrainment of air and the decrease in particle drag which has been observed when measurements were made of particle velocity in a cloud of particles in free fall.

FOREWORD

The research and development described in this document was conducted within the U.S. Department of Energy's (DOE) Solar Thermal Technology Program. The goal of the Solar Thermal Technology Program is to advance the engineering and scientific understanding of solar thermal technology, and to establish the technology base from which private industry can develop solar thermal power production options for introduction into the competitive energy market.

Solar thermal technology concentrates solar radiation by means of tracking mirrors or lenses onto a receiver where the solar energy is absorbed as heat and converted into electricity or incorporated into products as process heat. The two primary solar thermal technologies, central receiver and distributed receivers, employ various point and line-focus optics to concentrate sunlight. Current central receiver systems use fields of heliostats (two-axis tracking mirrors) to focus the sun's radiant energy onto a single tower-mounted receiver. Parabolic dishes up to 17 meters in diameter track the sun in two axes and use mirrors or Fresnel lenses to focus radiant energy onto a receiver. Troughs and bowls are line-focus tracking reflectors that concentrate sunlight onto receiver tubes along their focal lines. Concentrating collector modules can be used alone or in a multi-module system. The concentrated radiant energy absorbed by the solar thermal receiver is transported to the conversion process by a circulating working fluid. Receiver temperatures range from 100°C in low-temperature troughs to over 1500°C in dish and central receiver systems.

The Solar Thermal Technology Program is directing efforts to advance and improve promising system concepts through the research and development of solar thermal materials, components, and subsystems, and the testing and performance evaluation of subsystems and systems. These efforts are carried out through the technical direction of DOE and its network of national laboratories who work with private industry. Together they established a comprehensive, goal directed program to improve performance and provide technically proven options for eventual incorporation into the Nation's energy supply.

To be successful in contributing to an adequate national energy supply at reasonable cost, solar thermal energy must eventually be economically competitive with a variety of other energy sources. Components and system-level performance targets have developed as quantitative program goals. The performance targets are used in planning research and development activities, measuring progress, assessing alternative technology options, and making optimal component developments. These targets will be pursued vigorously to insure a successful program.

CONTENTS

ILLUSTRATIONS

TABLES

I. INTRODUCTION

Solid particles have been under consideration at Sandia National Laboratories, Livermore, as the working medium for a solar central receiver since the initial study was made by Martin and Vitko (1982). Falcone et al. (1982) provided a subsequent, favorable assessment of this concept in which particles in a size range from 100 to 1000 microns are transported from the ground to a solar receiver at the top of a tower. The particles then fall as a cloud or curtain through the receiver where they are irradiated directly by solar energy passing through the aperture of a cavity receiver. A conceptual design of a solid particle solar central receiver is shown in Figure 1. The solar energy is directed to the receiver by heliostats (mirrors) on the ground. Various materials have been considered for the solid particles including sand, Masterbeads (primarily aluminum oxide) made by the Norton Co., and silicon carbide. Proposed receiver designs consist of a cavity that is 5 to 10 meters tall with a single, side facing aperture.

Advantages of using a solid particle receiver over systems using conventional fluids such as water/steam are: (1) the particles absorb the concentrated solar flux directly, eliminating the need for a fluid conduit, (2) higher temperatures are possible, and (3) the particles can also serve as the storage medium, eliminating the need for additional piping and heat exchanger equipment.

In order to predict the temperature of the particles and the efficiency of energy absorption of the receiver, the following phenomena are addressed in the present work:

(1) radiation transport within the particle cloud and among the solid surfaces including the transport between the cloud and solid surfaces,

(2) two-phase flow of the air and the particles within the receiver, and

(3) convection heat transfer between the particles and the air and from the receiver surfaces.

Experimental Studies

In the experimental work of Hruby and Burolla (1984) concerning the flow of both heated and unheated particles from a hopper into ambient air, the particle volume fraction was small (less than 0.1 percent). and particle-particle collisions were infrequent except for a region near the hopper. This type of gas-particle flow is termed dilute, meaning that particle-particle collisions are not important. The gas-particle flow is expected to be dilute in the solid particle solar central receiver which contains particles in free fall. It is emphasized that characterizing the flow as dilute does not imply that coupling between

the phases is negligible. Air entrainment was shown to be important in the above experimental work in that velocities of the particles were significantly higher than the terminal values corresponding to an isolated particle falling in a quiescent environment. A separate experiment by Hruby et al. (1984) in which a radiant flux heated falling particles showed that the buoyant air resulted in an increase in the particle residence time (the time a particle remains within the radiant flux field). These experimental studies involving a cloud of particles falling in various thermal environments have shown that particle velocity, temperature, and residence time in such flows can only be predicted by including two-way momentum and thermal coupling (each phase providing significant source terms for the other phase) in the analysis.

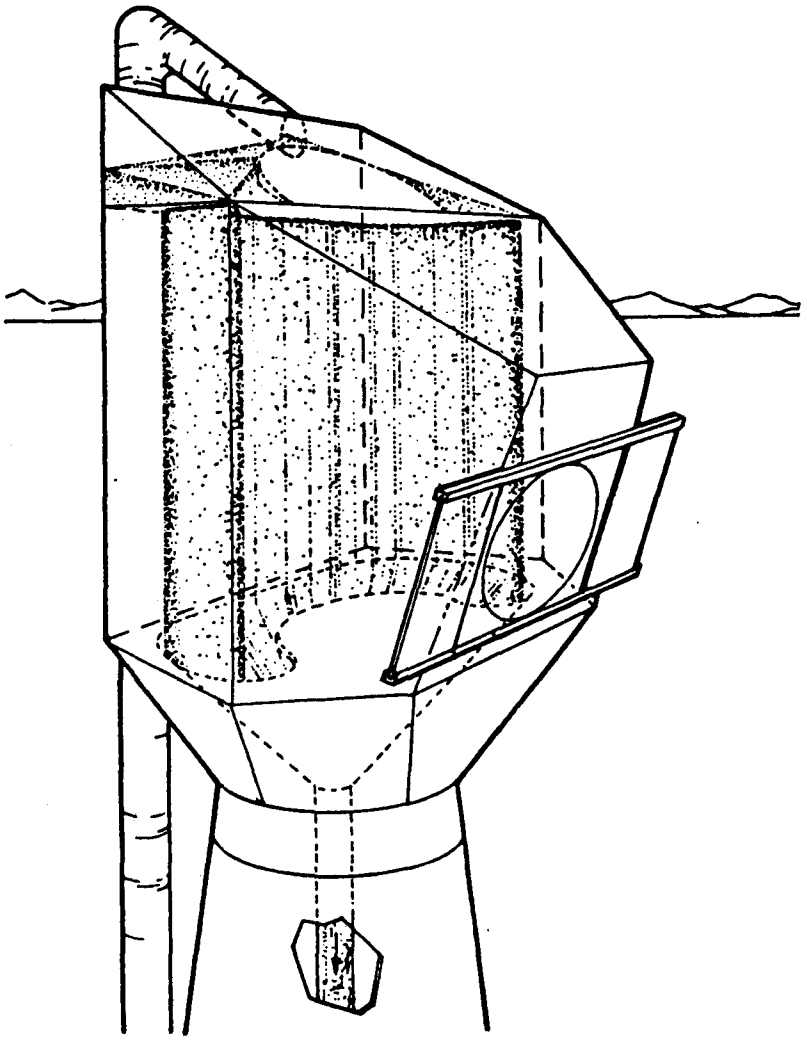

Figure 1. Conceptual design of a solid particle solar central receiver.

II. ANALYSIS

A model of dilute gas-particle flows with heat and mass transfer has been developed by Crowe et al. (1977). The model (PSI-Cell, i.e., Particle Source in Cell) has been applied to simulations of spray drying (Crowe, 1980), electrostatic precipitators (Eschbach and Stock, 1979), cyclone separators (Crowe and Pratt, 1974), and combustion (El-Bainhawy and Whitelaw, 1980). This report discusses the extension of the code to solid particle solar central receiver modeling by including gas buoyancy and radiation transport both within the particle cloud and among the cloud, the solid walls, and the aperture of the receiver. Briefly, the model consists of a steady, two dimensional, elliptic, Eulerian description of the gas flow field coupled with a Lagrangian description of the particle flow field. The gas flow field is determined using TEACHT (Gosman and Pun, 1973), which solves the conservation equations on staggered control volumes with the pressure, density, and temperature evaluated at control volume centers and the velocities evaluated at the control volume faces. A two equation (κ-ϵ) model of turbulence is included with constants established for a forced flow (Launder and Spalding, 1972). Convection and diffusion of a dependent variable are combined into a single term, which when integrated over the control volume, represents the flux of that variable across the faces of the control volume. These terms are evaluated using hybrid differencing (Spalding, 1972). This differencing scheme is a combination of central differencing and upwind differencing, switching from central to upwind when the absolute value of the cell Reynolds number is greater than two.

Gas Equations

The integrated forms of the conservation equations for mass, momentum, and energy are given by:

$$(\rho u)_w^e \cdot \Delta y + (\rho v)_s^n \cdot \Delta x = 0 \tag{1}$$

$$\left(\rho uu - \mu_{\text{eff}} \cdot \frac{\partial u}{\partial x}\right)_w^e \cdot \Delta y + \left(\rho vu - \mu_{\text{eff}} \cdot \frac{\partial u}{\partial y}\right)_s^n \cdot \Delta x = (P_w - P_e) \cdot \Delta y$$

$$- \rho g \cdot \Delta x \cdot \Delta y + \mu_{\text{eff}} \cdot \frac{\partial u}{\partial x}\bigg|_w^e \cdot \Delta y + \mu_{\text{eff}} \cdot \frac{\partial v}{\partial x}\bigg|_s^n \cdot \Delta x + {S_p}^x \tag{2}$$

$$\left(\rho uv - \mu_{\text{eff}} \cdot \frac{\partial v}{\partial x}\right)_w^e \cdot \Delta y + \left(\rho vv - \mu_{\text{eff}} \cdot \frac{\partial v}{\partial y}\right)_s^n \cdot \Delta x = (P_s - P_n) \cdot \Delta x$$

$$+ \mu_{\text{eff}} \cdot \frac{\partial u}{\partial y}\bigg|_w^e \cdot \Delta y + \mu_{\text{eff}} \cdot \frac{\partial v}{\partial y}\bigg|_s^n \cdot \Delta x + {S_p}^y \tag{3}$$

$$\left[\rho uT - \left(\frac{k}{c_p}\right)_{\text{eff}} \cdot \frac{\partial T}{\partial x}\right]_w^e \cdot \Delta y + \left[\rho vT - \left(\frac{k}{c_p}\right)_{\text{eff}} \cdot \frac{\partial T}{\partial y}\right]_s^n \cdot \Delta x = {S_p}^T \tag{4}$$

where e, w, n, s indicate that the corresponding terms are to be evaluated at the east, west, north, and south faces of the control volume, and Δx and Δy are the control volume dimensions in the x and y directions, respectively. The dissipation term in the energy equation is small and has been neglected. The source terms, ${S_p}^x$, ${S_p}^y$, and ${S_p}^T$, refer to the momentum and energy added to the gaseous phase by the particles. Additional equations and relationships for the gas flow solution are:

(1) pressure is determined using the SIMPLER procedure described by Patankar (1980) which is formulated to insure local continuity,

(2) differential equations for turbulent kinetic energy, κ, and dissipation, ϵ , are solved,

(3) effective viscosity and conductivity are given by

$$\mu_{\text{eff}} = \mu + \mu_{\text{turb}} \tag{5}$$

$$\mu_{\text{turb}} = c_\mu \rho \kappa^2 / \epsilon \ , \quad c_\mu = 0.09 \tag{6}$$

$$\frac{k_{\text{eff}}}{c_p} = \mu_{\text{eff}} \tag{7}$$

Equation (7) is the result of assuming that the effective Prandtl number is unity.

(4) an ideal gas equation of state is used and Sutherland law relationships for the dependence of viscosity and thermal conductivity on temperature are prescribed.

Particle Equations

The particle momentum and energy equations are given by:

$$\rho_p \cdot \frac{\pi {d_p}^3}{6} \cdot \frac{Du_p}{Dt} = 3\pi d_p \mu \lambda (u - u_p) - \rho_p \cdot \frac{\pi {d_p}^3}{6} \cdot g \tag{8}$$

$$\rho_p \cdot \frac{\pi {d_p}^3}{6} \cdot \frac{Dv_p}{Dt} = 3\pi d_p \mu \lambda (v - v_p) \tag{9}$$

$$\rho_p c_{p_{part}} \cdot \frac{\pi {d_p}^3}{6} \cdot \frac{DT_p}{Dt} = \text{Nu} k \pi d_p (T - T_p) + Q_{\text{rad}} \tag{10}$$

The determination and implementation of Q_{rad} is discussed separately. The particle velocity, position (trajectory), and temperature are calculated by integrating equations (8)-(10) from a prescribed starting location assuming initial particle velocity and temperature.

Gas Source Terms

The force in the x direction on the gas in the computational cell due to the particles is given by:

$$S_p{}^x = F_p{}^x \sum_i \dot{N}_i \Delta t_i \tag{11}$$

where $F_p{}^x$ is the aerodynamic force on the gas due to a particle, $\dot{N}_i$ is the particle number flow rate along the i^{th} trajectory, and Δt_i is the particle transit time across the cell for the i^{th} trajectory. The sum is applied over all trajectories passing through the computational cell for which the source term is being evaluated. A similar expression holds for the y direction source term. The energy equation source term for the gas is given by:

$$S_p{}^T = (Q_p/c_p) \sum_i \dot{N}_i \Delta t_i \tag{12}$$

where Q_p is the convection heat transfer rate from a particle to the air. Single particle drag coefficients and Nusselt number correlations are used:

$$F_p{}^x = \frac{C_D}{2} \cdot \rho \cdot \frac{\pi {d_p}^2}{4} \cdot |\vec{u}_p - \vec{u}| \cdot (u_p - u) \tag{13}$$

$$\lambda = C_D/C_{D_{\text{Stokes}}} = 1 + 0.15 \cdot \text{Re}^{0.687} \; ; \quad \text{valid for Re} \; \leq \; 10^3 \quad \text{(Wallis, 1969)} \tag{14}$$

$$Q_p = \text{Nu} \cdot k\pi d_p \cdot (T_p - T) \tag{15}$$

$$\text{Nu} = 2 + 0.6\sqrt{\text{Re}} \cdot \text{Pr}^{1/3} \quad \text{(Bird et al., 1960)} \tag{16}$$

Radiation Model

The radiation model used in this study considers the interaction of an incident radiation field with the falling particle cloud and receiver rear wall. The model accounts for the directional nature of the radiation field, particle scattering, thermal emission and the wavelength dependence of the particle optical properties. The equation which governs the radiation field within the particle cloud at any elevation is (Siegel and Howell, 1981):

$$\cos\theta \cdot \frac{dI_\lambda}{dy'}(y', \theta, \phi) = -(\sigma_\lambda + \kappa_\lambda) I_\lambda(y', \theta, \phi) + \kappa_\lambda I_{b,\lambda}(T_p)$$

$$+ \frac{\sigma_\lambda}{4\pi} \int\int_\Omega I_\lambda(y', \theta', \phi') p_\lambda(\theta', \phi' \rightarrow \theta, \phi) d\Omega \tag{17}$$

where the quantity $I_\lambda(y', \theta, \phi)$ is the monochromatic intensity at y' in the direction (θ, ϕ), and the subscript λ denotes wavelength. The depth, y', into the particle cloud at any elevation is measured from the edge of the cloud that is receiving the incident solar flux. The geometry for the radiative transport within the particle cloud is shown in Figure 2.

The intensity is the fundamental quantity that governs the radiation field within the particle cloud. The absorption coefficient, κ_λ, scattering coefficient, σ_λ, and phase function, $p_\lambda(\theta', \phi' \rightarrow \theta, \phi)$, are monochromatic optical properties which depend on the size, complex refractive index, and concentration of the particles in the cloud. The absorption and scattering coefficients characterize the attenuation per unit pathlength along a traversing beam of radiation due to the respective effects of scattering and absorption. The phase function represents the probability that a beam moving in the direction (θ', ϕ') and confined to a solid angle $d\Omega'$, will be scattered into a solid angle $d\Omega$ about the direction (θ, ϕ).

To simplify the presentation, the dimensionless parameters $\omega_\lambda = \sigma_\lambda/\beta_\lambda$ and $d\tau_\lambda = \beta_\lambda dy'$, are introduced where the extinction coefficient, β_λ, is the sum $(\sigma_\lambda + \kappa_\lambda)$. The quantity τ_λ is termed the optical thickness, and the total optical thickness of the cloud is defined as

$$\tau_{\lambda,d} = \int_0^d \beta_\lambda dy' \tag{18}$$

where d is the thickness of the particle cloud at a particular elevation. The total optical thickness, $\tau_{\lambda,d}$, is a measure of the ability of the particle cloud to attenuate radiation of a given wavelength. The quantity ω_λ is the single scattering albedo and is a measure of the relative importance of scattering to absorption in the interaction of radiation with a single particle. The albedo ranges from a value of zero for a purely absorbing particle, to a value of one for a particle that only scatters radiation. If the optical properties and lateral temperature profile for the solid carriers are known, then the radiative transfer equation can be solved subject to boundary conditions at the front and rear of the particle cloud to determine the intensity $I_\lambda(y', \theta, \phi)$. Knowing I_λ, the forward (for) and backward (bac) components of the local spectral radiative heat flux can then be determined from the following expressions:

$$F_{\lambda,\text{for}}(y') = \int_0^{2\pi} \int_0^{\pi/2} I_\lambda(y', \theta, \phi) \cos\theta \sin\theta d\theta d\phi \tag{19}$$

$$F_{\lambda,\text{bac}}(y') = \int_0^{2\pi} \int_{\pi/2}^{\pi} I_\lambda(y', \theta, \phi) \cos\theta \sin\theta d\theta d\phi \tag{20}$$

The total spectral radiative flux, F_λ, is the sum

$$F_\lambda(y') = F_{\lambda,\text{for}} + F_{\lambda,\text{bac}} \tag{21}$$

The total radiative flux is then determined by integrating the monochromatic flux over the entire spectrum; that is

$$F(y') = \int_{all\ \lambda} F_\lambda(y')\ d\lambda \tag{22}$$

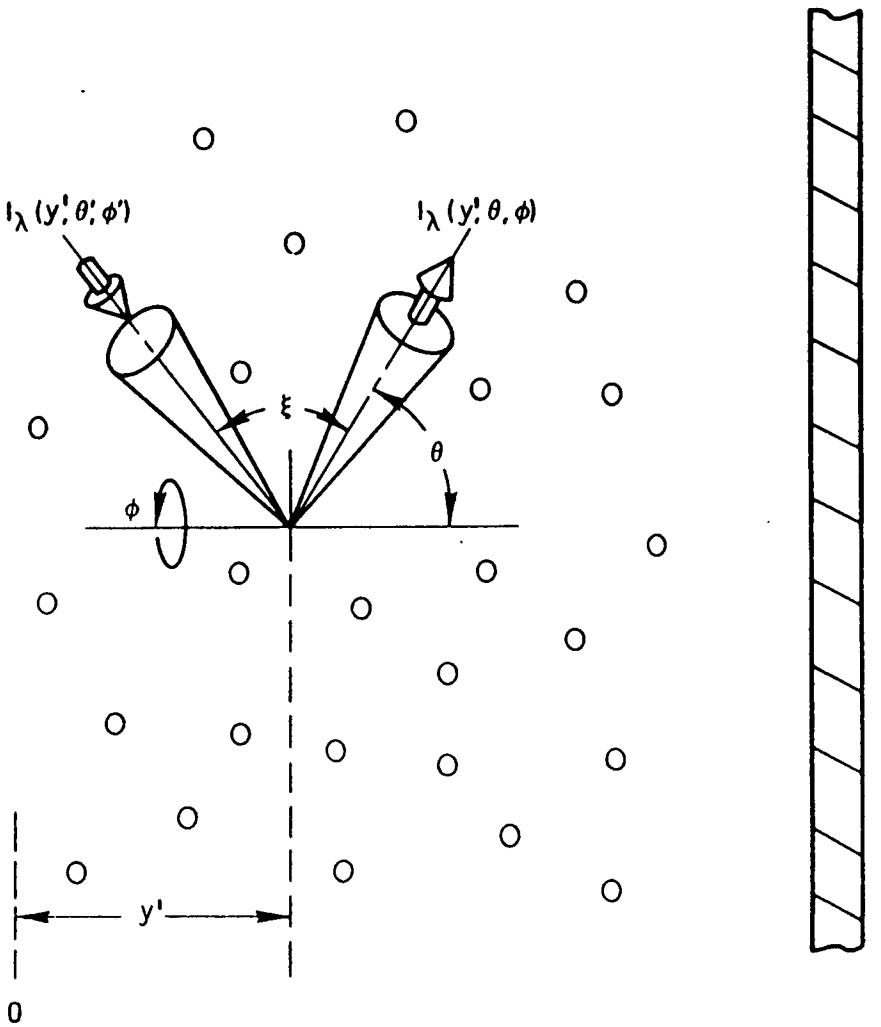

Figure 2. Radiative transfer geometry.

The method of discrete ordinates is an accurate solution technique which has been applied to radiative transfer problems; it is the approach used in this study. The details of the method are given elsewhere (Houf and Greif, 1985) and will not be repeated here. For the purposes of this study, the scattering distribution, $p_\lambda(\theta', \phi' \rightarrow \theta, \phi)$, was represented by a function of the form

$$p(\xi) = 1 + \sum_{k=1}^{100} (2k+1) g^k P_k(\cos\xi) \tag{23}$$

where the P_k are Legendre polynomials of order k, and ξ is the angle between the incident (θ', ϕ') and scattered beams (θ, ϕ). The value g is an asymmetry factor which varies from -1 (strictly backward scattering) to 1 (strictly forward scattering). A value of g equal to 0, which corresponds to an isotropic scattering distribution, is used in this study. Calculations over the range $g = -0.5$ to $g = 0.5$ show a variation of 15 percent in the absorbed solar radiation for a typical set of conditions (Houf and Greif, 1985).

Solution Method

The numerical solution is iterative and consists of the following steps:

1. The air flow field within the receiver is first determined for a specified solar heat flux in the absence of particles.

2. Particles are then introduced from a point source at the top of the receiver. Particle velocity, temperature, and position are determined by integrating equations (8)-(10).

3. The horizontal thickness, d, of the particle cloud at each elevation corresponding to a computational cell boundary for a scalar quantity in the gas is determined from the locations of the front and rear trajectories. Average particle number density, n, and an average particle temperature are determined at these horizontal locations (the radiation transfer within the particle cloud may also be determined for variable particle temperature but this feature is not used in the present study).

4. The radiative transport equation is solved for each horizontal slice (of vertical extent Δx) of the particle cloud; the incident irradiation at the front edge of the cloud and the reflectivity of the back wall are specified.

5. Particle temperatures are then recalculated with radiation source terms obtained from the solution of the radiative transport equation (step 4), where Q_{rad} for a particle between y' and $y' + \Delta y'$ is calculated from:

$$Q_{\text{rad}} = \frac{[F(y') - F(y' + \Delta y')]}{n \cdot \Delta y'} \tag{24}$$

Iteration between this step and the preceding one is continued until there is a relatively small change in particle temperature. Gas source terms are then accumulated.

6. The conservation equations for the gas are now solved including the source terms due to the particles. Boundary conditions for the energy equation for the gas are obtained by making wall element energy balances including radiation, convection, and a specified amount of conduction through the wall along with the Reynolds analogy for the specification of the heat transfer coefficient. These wall energy balances are embedded within a radiation enclosure calculation consisting of thermal radiation transport among all the receiver surfaces and with the front of the particle cloud. From this enclosure calculation, a new irradiation on the front of the particle cloud is then determined.

7. Steps 2 to 6 are repeated until convergence criteria based on the total residuals of the mass, momentum, and energy equations of the gas are obtained. For each equation the total residual is determined as the sum of the absolute value of the local residuals over all control volumes. Since the equations are in dimensional form, the convergence criteria are also dimensional. The values used are 0.01 kg/s for the total mass residual, 1.0 Nt for the total momentum residual, and 4.0 kg-K/s for the total energy residual. Dividing these convergence criteria by the number of control volumes and normalizing by the magnitude of a characteristic term in the equations gives a measure of the relative error. For the above convergence criteria, this error is $4x10^{-5}$ for the continuity equation, $4x10^{-3}$ for the momentum equation, and 10^{-4} for the energy equation. Negligible changes in the dependent variables occurred at a monitoring location when the above values were satisfied simultaneously.

III. NOMINAL CAVITY CALCULATIONS AND DISCUSSION

Geometry and Boundary Conditions

The base case solid particle receiver geometry used in modeling is shown in Figure 3. The receiver consists of a two dimensional, rectangular cavity that is 5 m deep and 6.7 m high. An aperture to allow for the incident solar flux is 4.1 m high, and an opening of 1.1 m at the top is used for the introduction of the particles. Air enters the cavity through the aperture at 293 K. The particle mass flow is introduced as a point source at the top of the cavity ($x = 6.7$ m, $y = 1.25$ m), with the mass flow rate divided into ten equal parts. Since the model is two dimensional, the mass flow rate is given with units of kg/(s - meter width of cavity). The particles are given an initial downward speed of 0.3 m/s and an initial temperature of 293 K. An initial spray cone of 0.6 radian is applied. These initial conditions for the particle velocity were inferred from the spread rates of particles falling from a hopper into ambient air in the experimental work of Hruby and Burolla (1984). Zero gradient conditions for the dependent variables are set at the top outflow opening. A hydrostatic pressure gradient is imposed between the aperture and the top opening ($\Delta P = \rho_\infty g L$). A provision is made for applying a back pressure at the top opening by modifying the hydrostatic pressure at this position with the constant, K, where $\Delta P = K \rho_\infty g L$. Values of K less than 1.0 are used to simulate the effects of a pressure drop caused by heat exchanger or particle distribution equipment placed over the top opening. Zero pressure correction and a direct application of the continuity equation are used across the fluid inlet and outlet areas in order to obtain velocities across these planes.

Typical computer time on a Cray-1 varied from 5 to 10 minutes. The original version of the code used the SIMPLE (Patankar, 1980) algorithm to satisfy continuity and to compute the pressure field. By incorporating SIMPLER (Patankar, 1980), which allows for an additional equation for the pressure field, the number of iterations required to reach a converged solution was reduced by a factor of 8, and the computational time was reduced by a factor of 4.

Nominal Parameter Values

The following nominal parameter values were used in the calculations: 0.92 MW/m^2 incident solar energy (uniformly applied to the front of the cloud), 5.4 kg/s particle mass flow rate, 650 micron diameter, spherical, bauxite particles, particle density of 3130 kg/m^3 and temperature dependent specific heat, initial particle temperature and downward velocity of 293 K and 0.3 m/s, a two band radiation calculation with a solar band from 0.2 to 1.5 microns and an infrared band from 1.5 to 30 microns, particle scattering albedo of 0.12 in the solar band and 0.4 in the infrared band (Stahl et al., 1985), and cavity

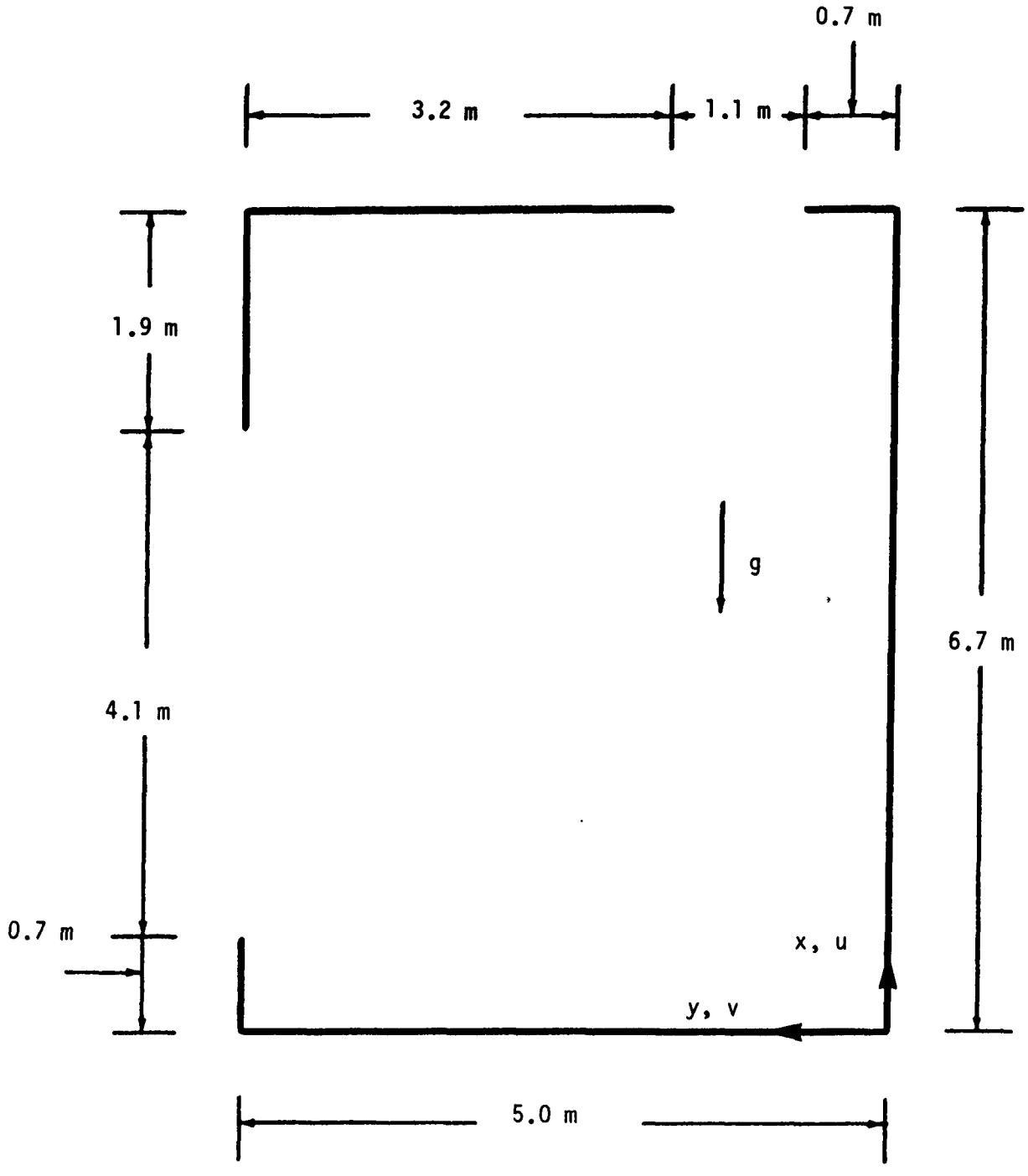

Figure 3. Solid particle receiver geometry.

wall reflectivity of 0.2 for both bands. Cavity wall temperatures were determined from a radiation enclosure calculation within the cavity.

Air and Particle Fields

Figures 4a and 4b show the calculated air flow field with and without particles, respectively, for the conditions described above. The air flows in the aperture, turns upward at the hot back wall of the cavity, and flows out of the opening at the top. A significant increase in upward air movement occurs as a result of the buoyancy generated by the convective heat transfer from the particles. In the lower section of the cavity, entrainment of cold air into the falling particle cloud is shown by the downward motion of the air. Isotherms in the interior of the cavity are shown in Figures 5a and 5b, with and without particles, respectively. The convection from the particles to the air is evident in the lower portion of the cavity where the cold inflowing air interacts with the hot falling particles.

Particle temperatures for the extreme (front and back) trajectories are shown in Figure 6 as a function of vertical position within the cavity. For this mass flow rate of 5.4 kg/s, the optical thickness, $\tau_{\lambda,d}$, of the particle cloud varies from a value of 3 near the particle inlet at the top of the cavity to 0.5 at the bottom of the cavity. A temperature difference of approximately 400 K from the front to the rear particle trajectory results over much of the fall height of the particles. In a study of the radiative transfer within the particle cloud at a fixed wavelength, Houf and Greif (1985) showed that as the optical thickness of the particle cloud increases, the ratio of radiative absorption between the front and the back of the particle cloud increases. Furthermore, the fraction of incident solar energy absorbed increases. Particle vertical velocities for the front and rear trajectories are shown in Figure 7 (negative velocity corresponds to downward motion). At a given elevation there is very little variation in velocity. The change in slope of the vertical velocity along the front trajectory (traj. 1) which occurs approximately 3 m from the top opening is a result of the large grid spacing. As the particles approach the cavity bottom they attain a terminal velocity slightly greater than 7 m/s. The terminal velocity for an isolated particle falling in a stationary ambient medium at atmospheric pressure and with a temperature of 500 K (average conditions in the cavity) is less than 6 m/s, which indicates that the particles are entraining air as they fall through the cavity.

Mesh Refinement and Wall Function Application

The results described above were computed on a uniform, coarse mesh using 20 grid lines in the vertical (x) direction and 16 grid lines in the horizontal (y) direction. The values of Δx and Δy were 0.37 m and 0.36 m, respectively. Wall functions developed for turbulent forced flows near bounding surfaces (Launder and Spalding, 1972) were used to provide a wall shear stress source term for the gas at the first computational control volume away from the wall. Instead of making calculations in the viscous sublayer, wall functions were used because the large number of grid points required to resolve the boundary layers to this level has an adverse impact on the convergence properties of the code (Alpert, 1984; Launder, 1984). It is also noted that the (κ-ϵ) turbulence model being used would have

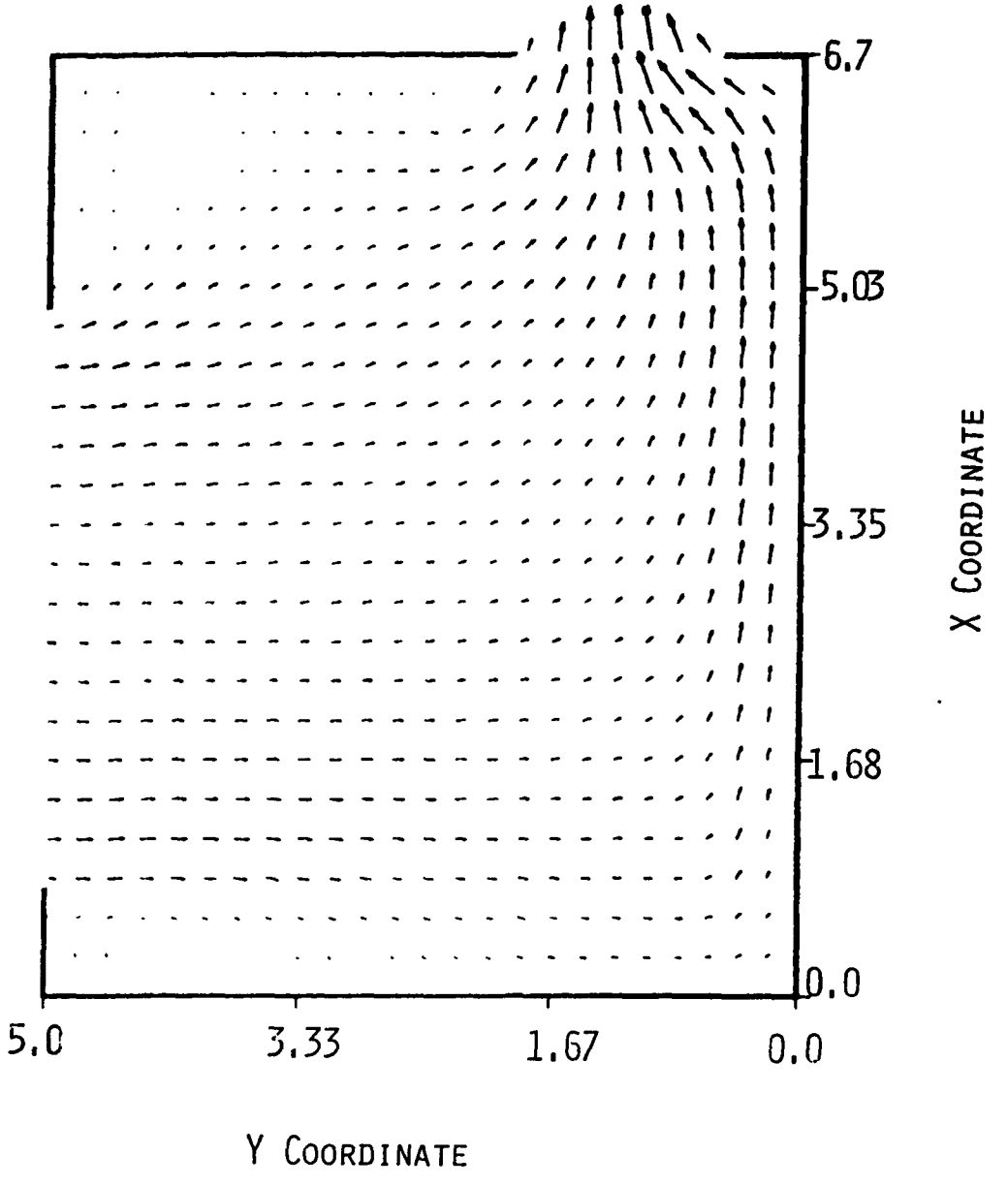

Figure 4a. Air flow field without particles. The maximum air velocity is 2.5 m/s.

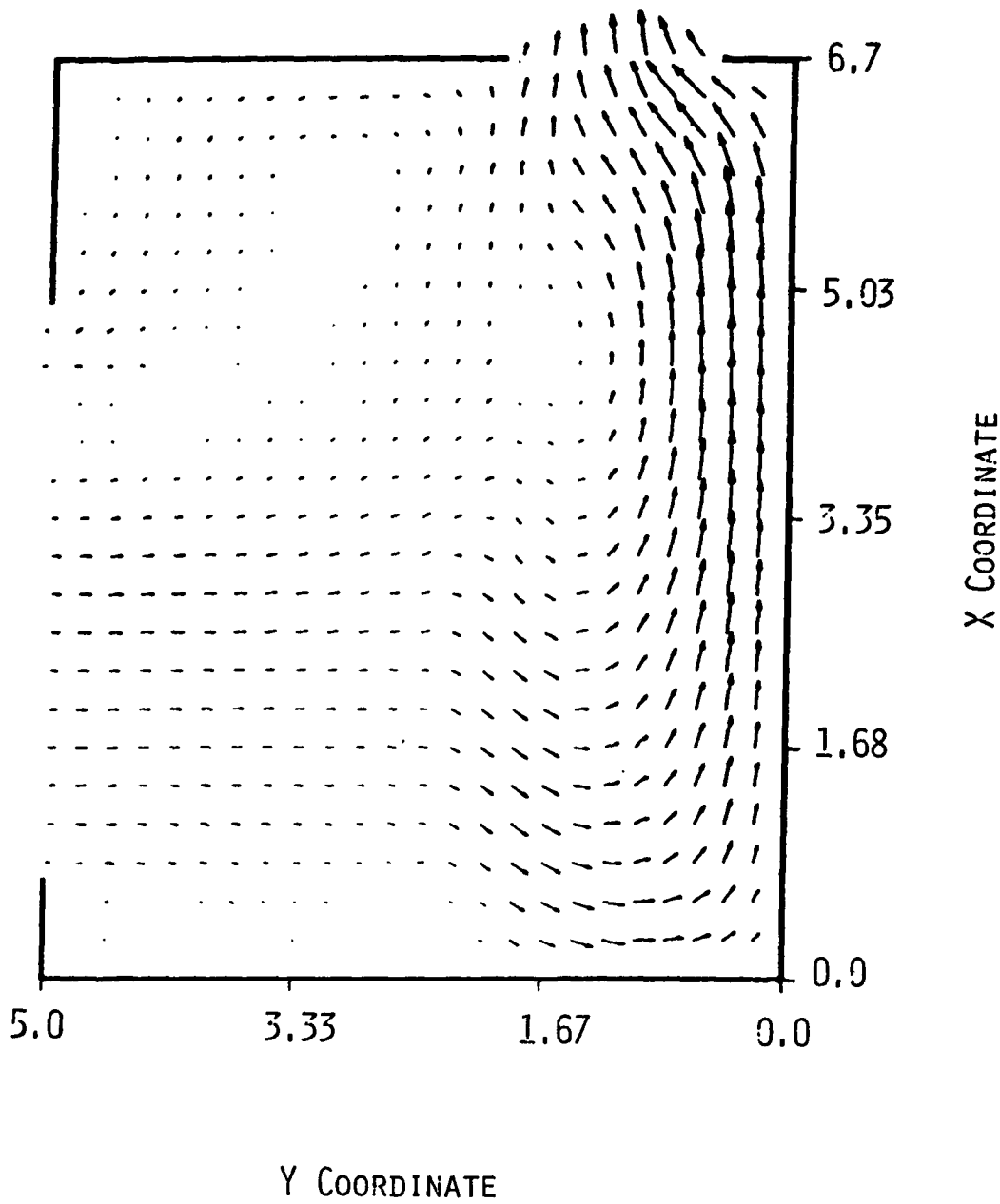

Figure 4b. Air flow field with particles. The maximum air velocity is 8.9 m/s.

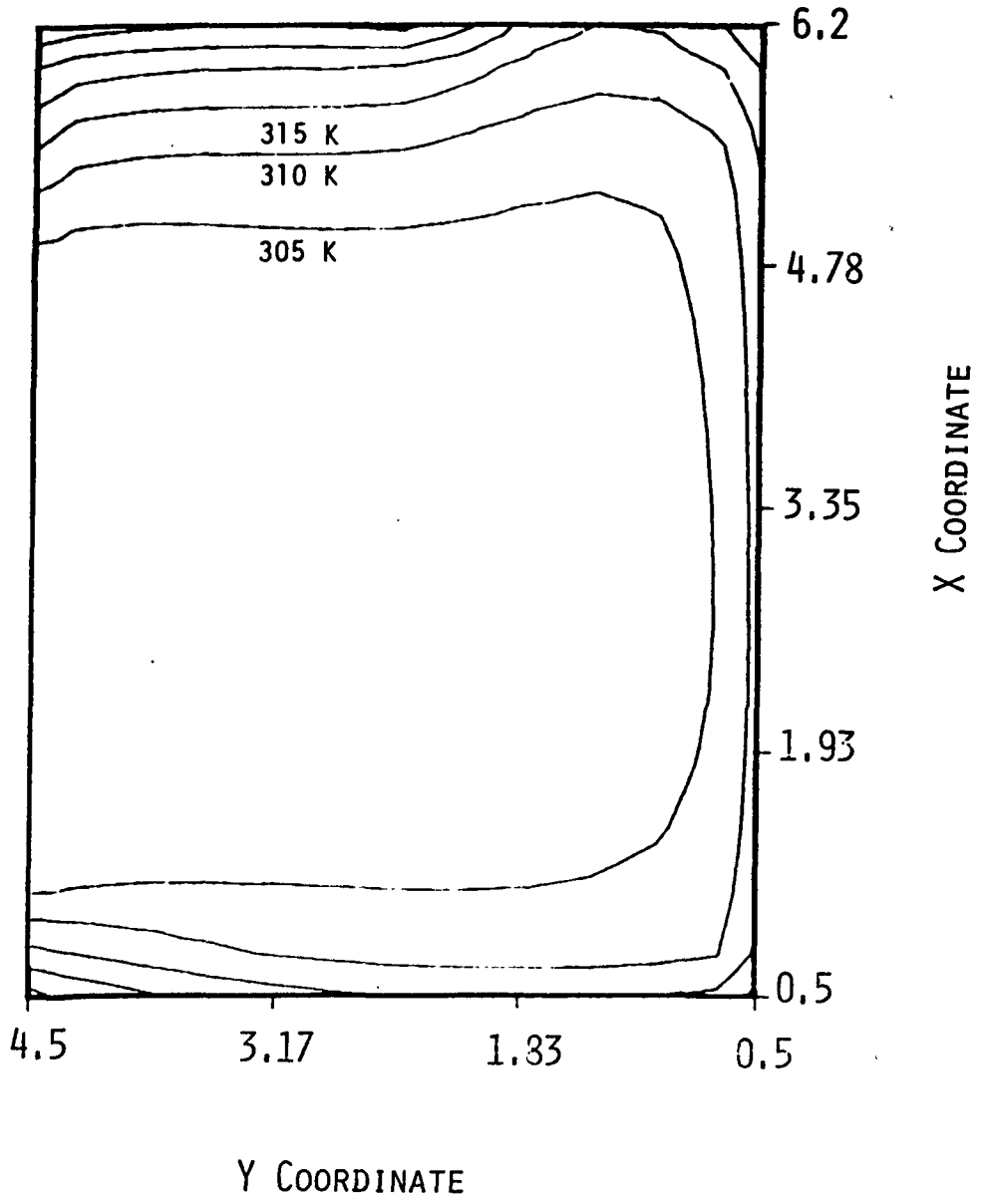

Figure 5a. Air isotherms without particles.

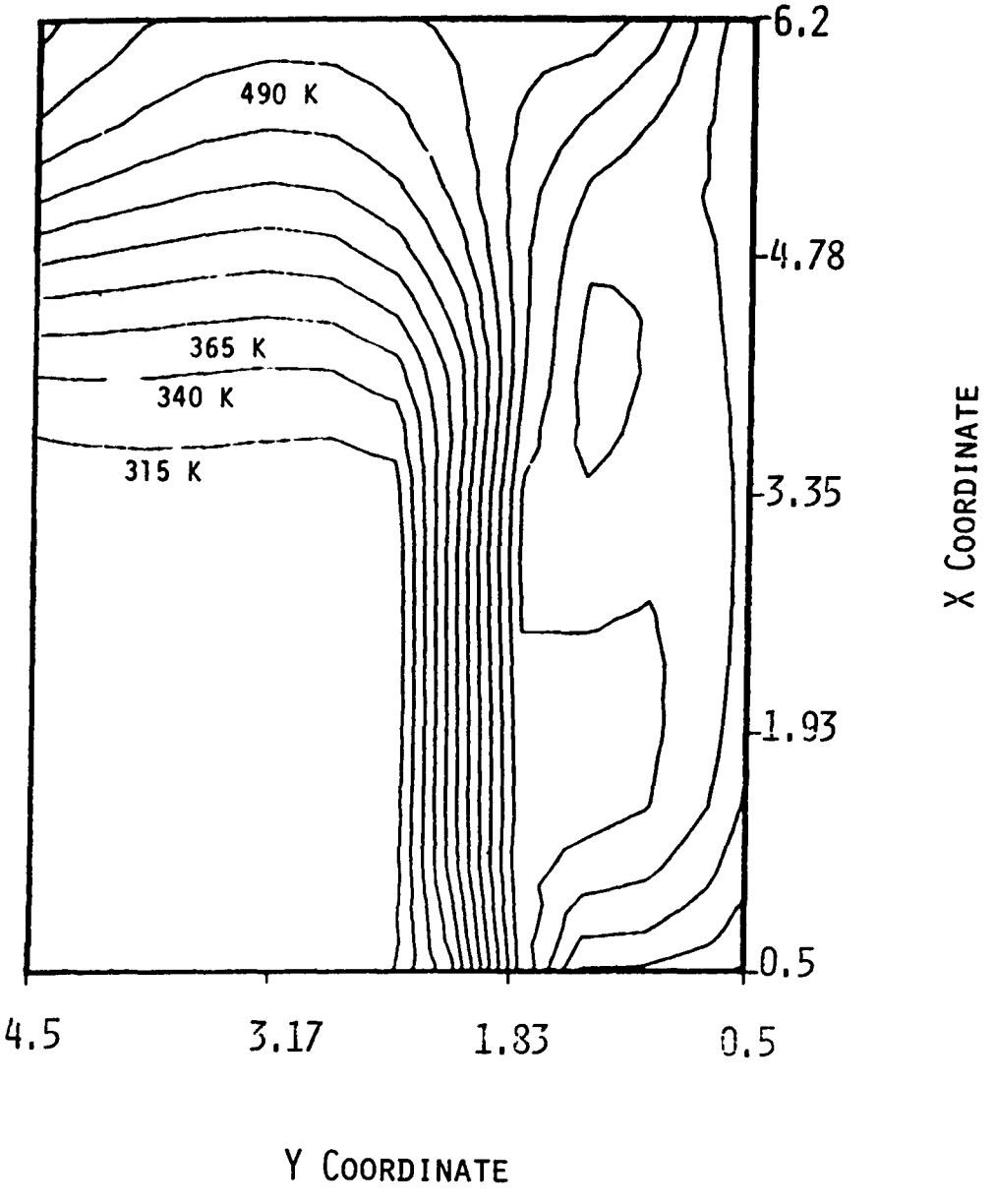

Figure 5b. Air isotherms with particles.

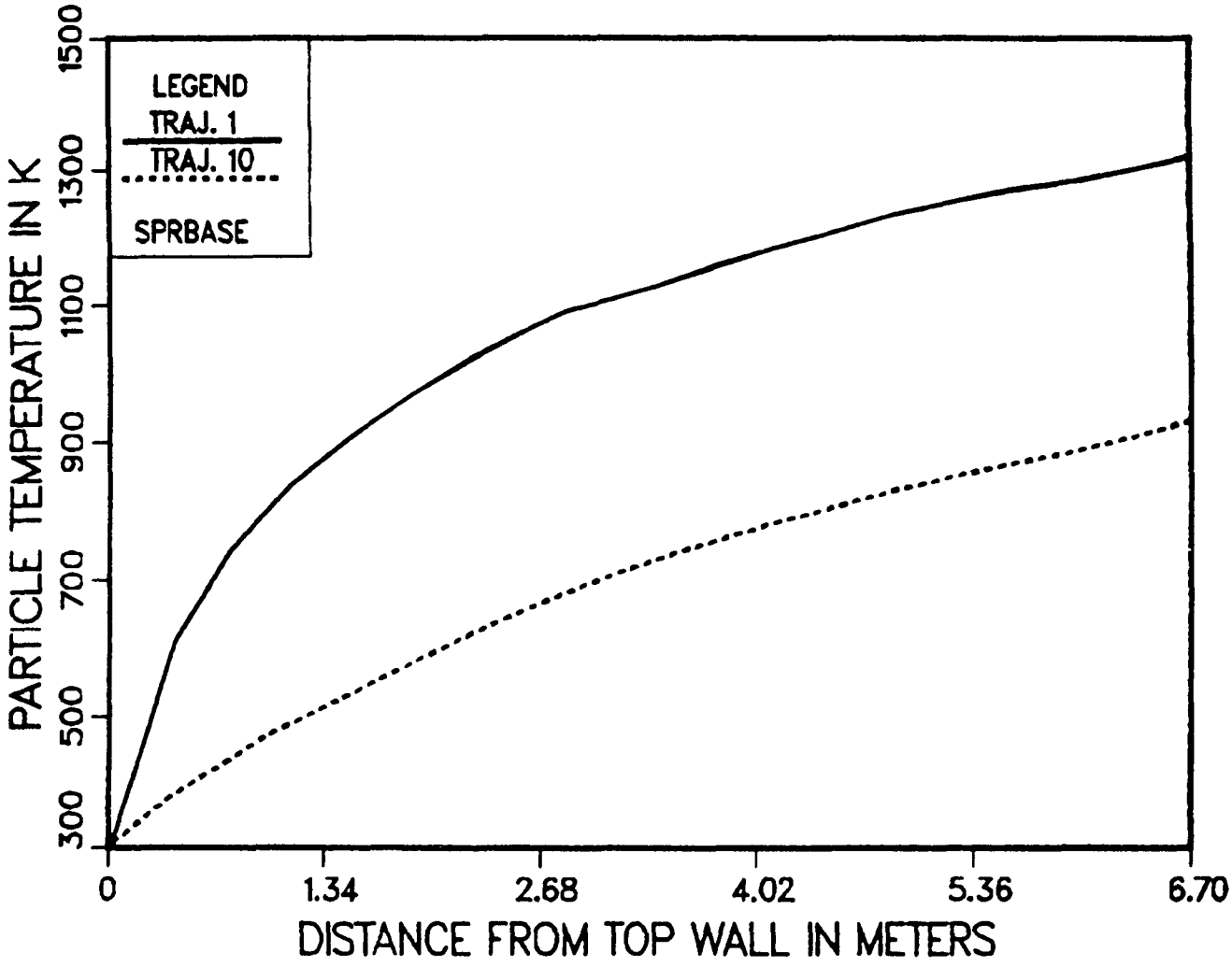

Figure 6. Particle temperatures for the front (no. 1) and back (no. 10) particle trajectories as a function of vertical position in the cavity.

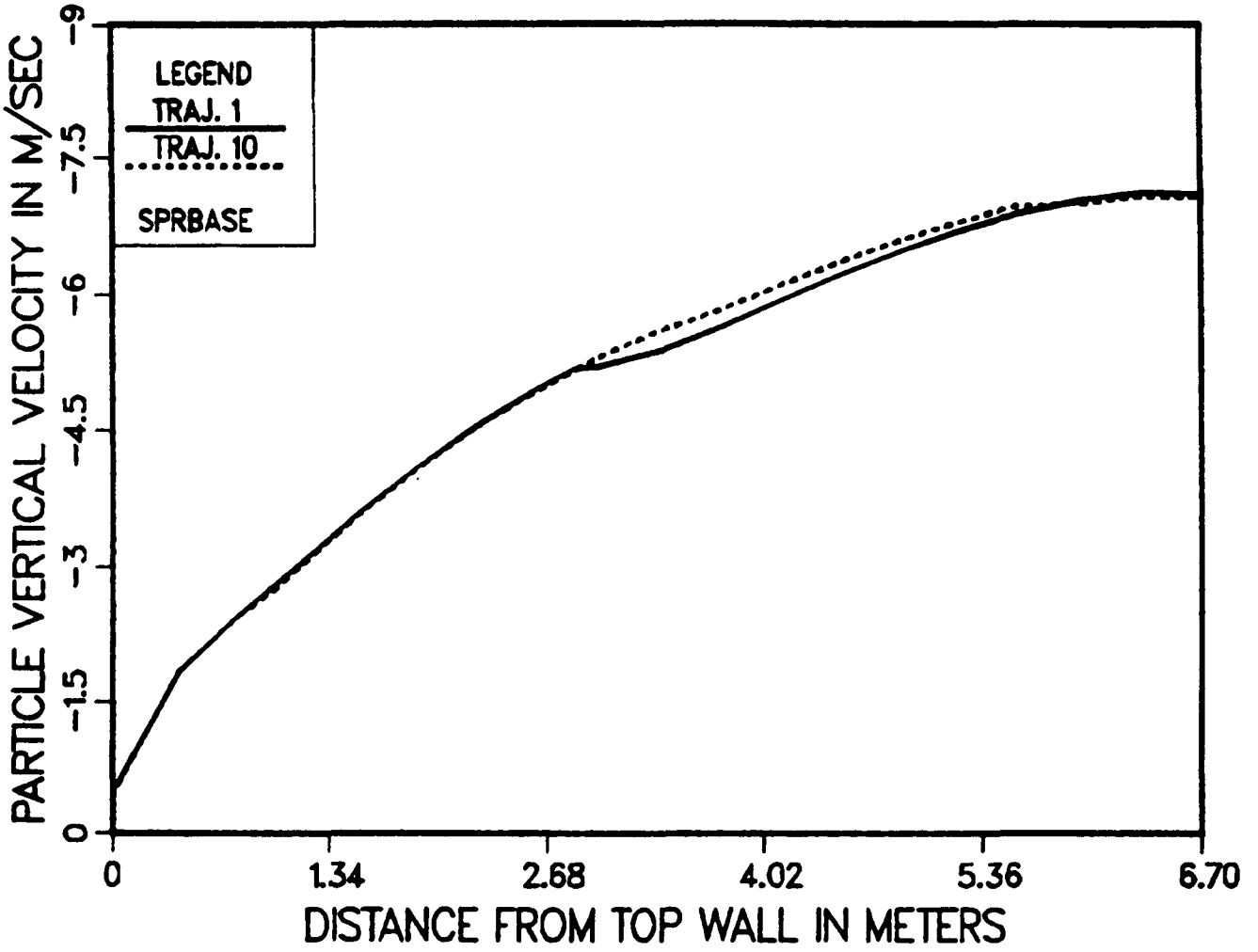

Figure 7. Particle vertical velocities for the front (no. 1) and back (no. 10) particle trajectories as a function of vertical position in the cavity.

required modifications to account for viscous and wall damping effects in the near wall region. Although the κ-ϵ turbulence model of Jones and Launder (1972) has been used by Plumb and Kennedy (1977) and Humphrey et al. (1985) (with modifications for buoyant effects) in calculating the turbulent natural convection boundary layer adjacent to a vertical, isothermal flat plate in a quiescent, unstratified ambient medium, the appropriate modifications in recirculating regions of a buoyant cavity flow have not been established.

For the uniform, coarse mesh of 16 by 20 grid lines, the distance from the wall to the first grid point is greater than the thickness of a turbulent natural convection boundary layer adjacent to a vertical, isothermal flat plate in an undisturbed ambient medium. The derivation of the wall function restricts its use to the logarithmic region of a turbulent wall flow. The logarithmic region of a forced turbulent boundary layer extends from a dimensionless distance, y^+, of 35 to 350 (White, 1974). Assumptions used in deriving the wall function are that the layer next to the wall is one of constant shear stress and that the production and dissipation of turbulent kinetic energy are in balance (convection and diffusion of turbulent kinetic energy are neglected). These assumptions imply that the point in question be relatively near the wall. However, the location of the first control volume next to the wall should be outside the viscous sublayer.

In addition to the uniform, coarse mesh calculations discussed above, the system of equations was also solved using a highly nonuniform grid (47 by 53 grid lines) such that all control volumes adjacent to walls had values of y^+ less than 100. Although the convergence criteria based on the total residuals of the mass, momentum, and energy equations which were attained for the coarse grid could not be fully achieved on this fine grid, the iterations were continued until the results for the velocity and temperature profiles showed little change (less than 0.5 percent). The resulting velocity field in the cavity without particles is shown in Figure 8 and can be compared to the corresponding coarse grid velocity field in Figure 4a. A larger recirculation zone can be seen below the lower lip of the cavity for the fine grid case. Also, the fine grid result shows some outflow from the cavity aperture which was absent in Figure 4a. With respect to the parameters of interest for the solid particle receiver, particle exit temperatures for the two cases differ by less than 20 K and the calculated cavity efficiency agrees to within 2 percent. Hence, the uniform coarse mesh was used in subsequent calculations.

Effects of Turbulence

The κ-ϵ turbulence model used in this analysis has been developed for forced flows in the absence of particles. Various researchers have modified this model to include the effects of buoyancy. However, Mason and Seban (1974) calculated a turbulent natural convection boundary layer adjacent to an isothermal vertical flat plate using the turbulent kinetic energy equation for a forced flow along with a prescribed length scale. The results obtained were in reasonable agreement with experimental profiles of the velocity and temperature. Abdelmeguid and Spalding (1979) used the κ-ϵ model with constants established for a forced flow to calculate the flow and heat transfer in a vertical pipe with buoyancy effects. They also obtained reasonable agreement with experimental results for the mean velocity and temperature profiles.

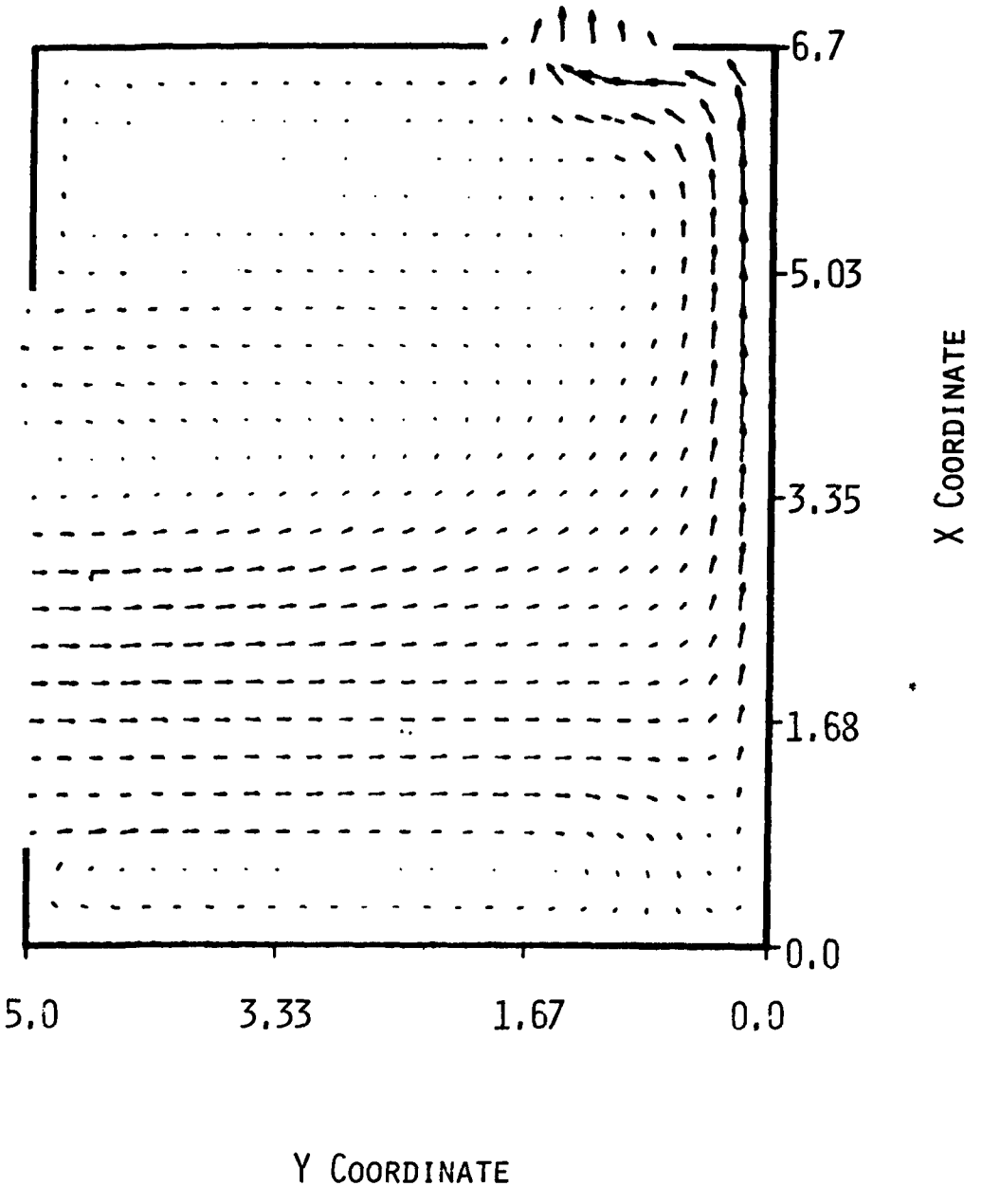

Figure 8. Air flow field without particles, computed on a 47×53 nonuniform grid. The maximum air velocity is 3 m/s.

Little information is available on the effect of the particles on the turbulence of the air. Injection of particles within a turbulent boundary layer has been shown to cause a reduction in wall drag. Results of various boundary layer investigations have been summarized by Rudinger (1980). However, in the present study, the particles are not confined to wall boundary layer regions. Soo (1967) has shown that particles have little effect on the turbulence of the air up to mass loadings, m_p/m_{air} , of at least 0.06. It is not clear what effect particles would have on the air turbulence for a mass loading close to unity which would be typical in a solid particle receiver.

As noted earlier, ten particle trajectories were used in the preceding calculations. The computed results were found to be insensitive to the number of trajectories used over a range from 5 to 20. The computed horizontal thickness of the particle cloud, d, was several centimeters and this thickness did not vary significantly over the fall height of the particles from the top to the bottom of the cavity. The particle motion as described by equations (8) and (9) is affected by the turbulence in the air only through the mean air velocity. There is no effect on the particle motion due to the random turbulent fluctuations. A method of determining particle dispersion in a turbulent flow field was described by Chen and Crowe (1984), who used a Monte Carlo approach to model the randomness of the turbulent gas field as seen by the particles. Briefly, the method consists of integrating the particle motion equations (8) and (9), with the gas velocity replaced with an average and a fluctuating part. The fluctuating gas velocity (with zero mean) is determined from the turbulence kinetic energy of the gas flow field, using a random number generator. The particle motion is affected by a particular fluctuating gas velocity for a time that is the minimum of either the characteristic eddy time of the gas turbulence or the time for the particle to pass through the eddy. A large number of particles is selected to provide a meaningful description of the dispersion of the particle cloud.

The Monte Carlo method was incorporated into the solid particle receiver computer code and 1000 trajectories were calculated. The results were consistent with those obtained using a deterministic approach, suggesting that for the present conditions, the particle motion is not altered significantly by the turbulent fluctuations of the air.

IV. PARAMETRIC EVALUATION OF RECEIVER

Effect of Varying Particle Parameters

Parameters were varied independently to determine their effect on cavity efficiency and particle exit temperature. Figure 9 shows the effect of varying the mass flow rate of the particles on the average exit temperature of the particles and on the efficiency of the cavity, defined as the ratio of the sensible energy gain of the particles to the incident solar energy. Increasing the particle mass flow results in an increase in cavity efficiency with a decrease in particle temperature. For a fixed incident flux, an energy balance shows that an increase in the mass flow rate leads to a decrease in the maximum temperature difference.*

Reducing the particle size is expected to increase both the cavity efficiency and particle temperature, since smaller particles result in a greater optical thickness (for a specified mass flow rate) and also remain in the flux field longer due to their smaller fall velocities. This does occur as shown in Figure 10, but the effect is not large. The convective heat transfer from the particles to the air increases as the particle size is reduced, and this effect partially offsets the gain in efficiency and limits the increase in the particle temperature as noted above. In Figure 11, the convective loss fraction, defined as the ratio of the total convective heat transfer between the particles and the air to the incident solar energy, is shown as a function of particle size.

The effect of using selectively absorbing particles was investigated by assigning one value of the particle scattering albedo, defined as the ratio of scattering to the sum of absorption and scattering, for the incident solar energy and another value for the reradiated energy from the cavity walls. By using a larger value of the scattering albedo for the infrared energy, the particles emit less energy and thus might be expected to retain a larger amount of the absorbed solar energy. However, as shown in Figure 12, both cavity efficiency and particle temperature decrease as the infrared scattering albedo increases. This is a result of the decreased absorption of the (large amount of) infrared energy emitted from the cavity walls which is incident on the particle cloud.

Figure 13 shows the effect of varying particle absorptivity, defined here as one minus the single scattering albedo defined earlier, on the cavity efficiency and on the average exit temperature of the particles. The results shown in this figure were calculated assuming that the radiative properties of the particles were independent of wavelength (gray particles). An additional parameter study involving radiative properties was performed in which the reflectivity of the cavity walls was varied from 0.2 to 0.9. There was negligible change in the efficiency of the cavity and the average exit temperature of the particles for this range

* Strictly, this would be valid for a fixed absorbed energy.

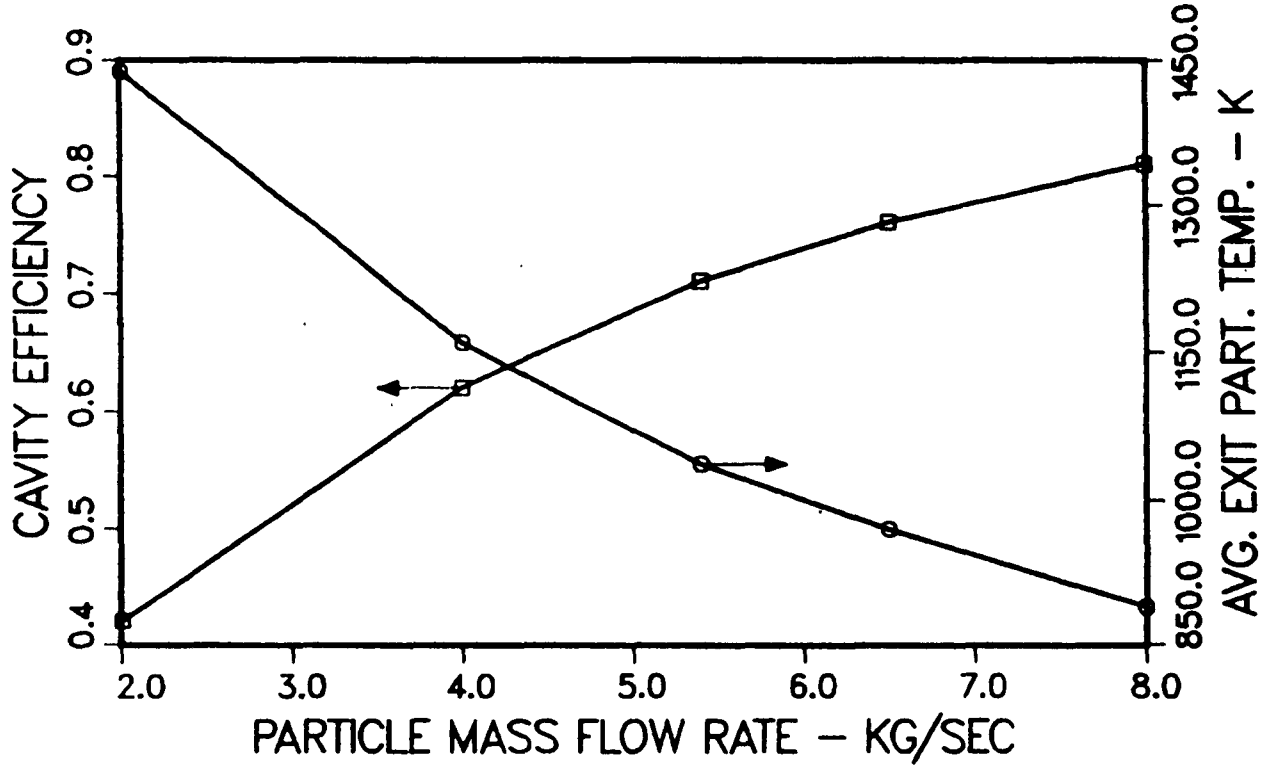

Figure 9. Variation of cavity efficiency and average exit temperature of particles as a function of mass flow rate of particles.

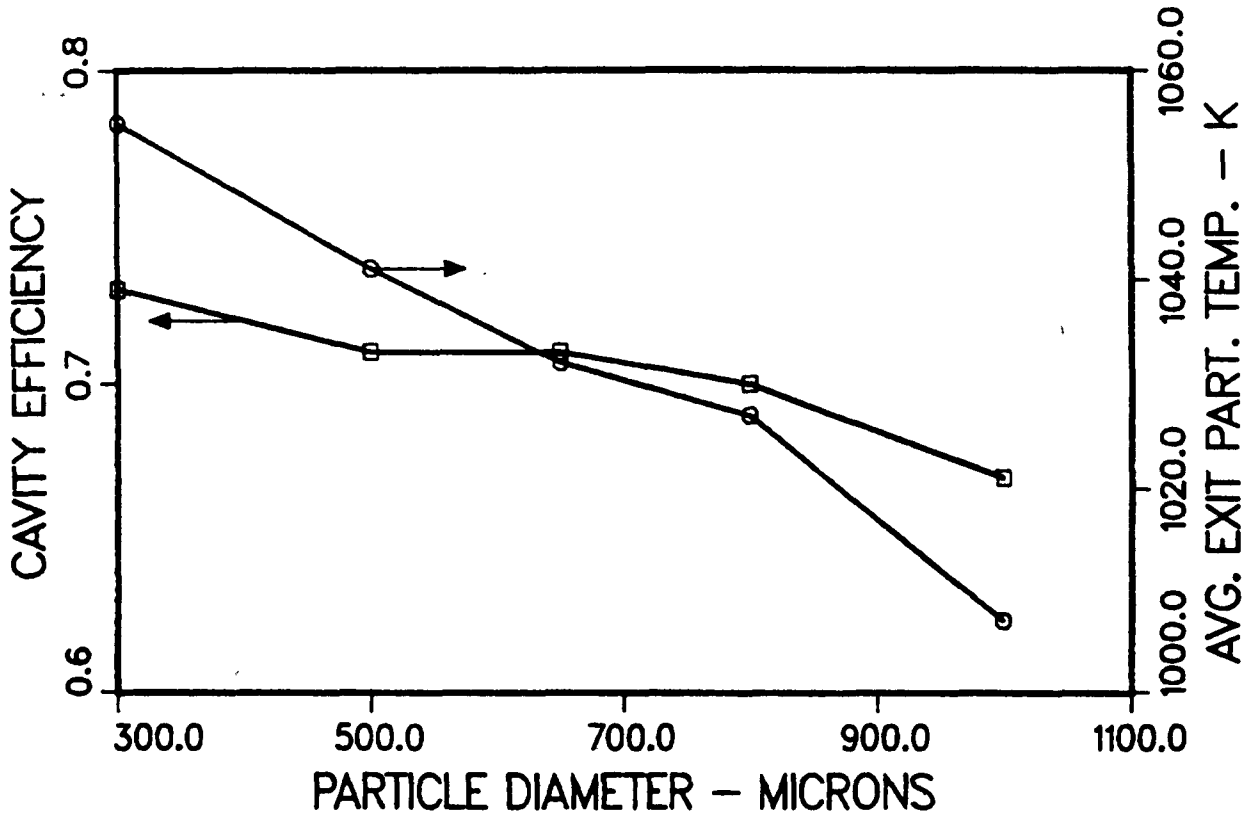

Figure 10. Variation of cavity efficiency and average exit temperature of particles as a function of particle size.

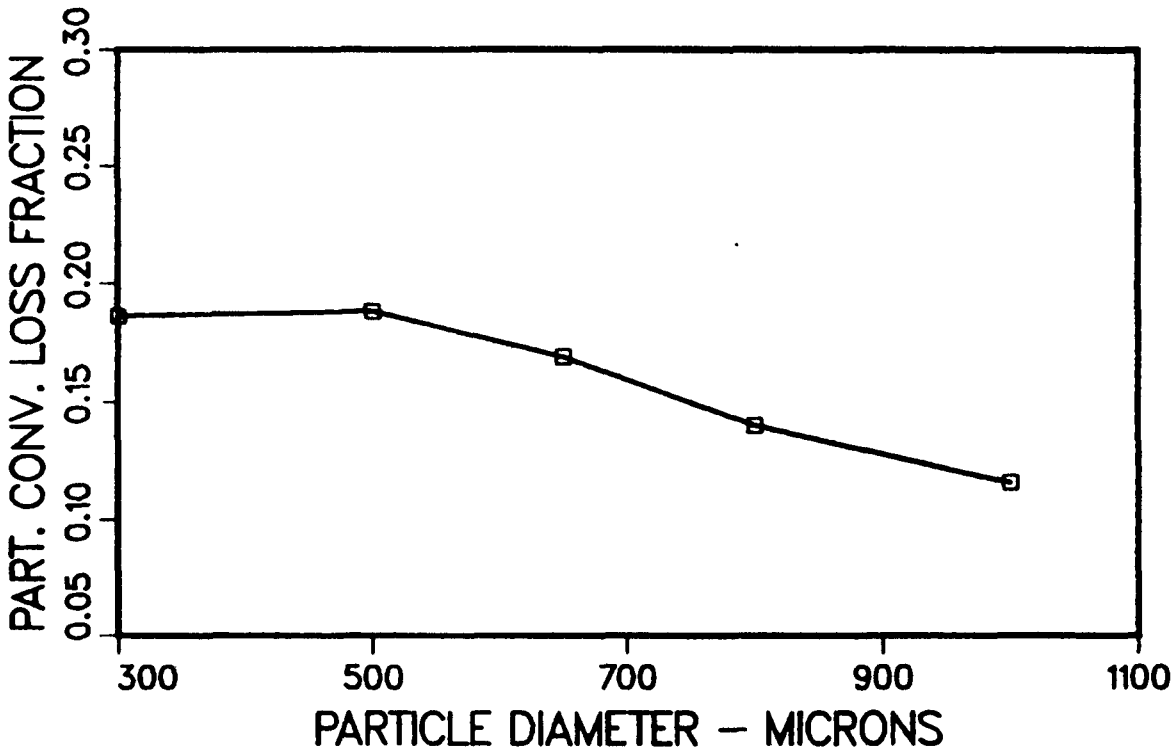

Figure 11. Variation of particle convective loss fraction as a function of particle size.

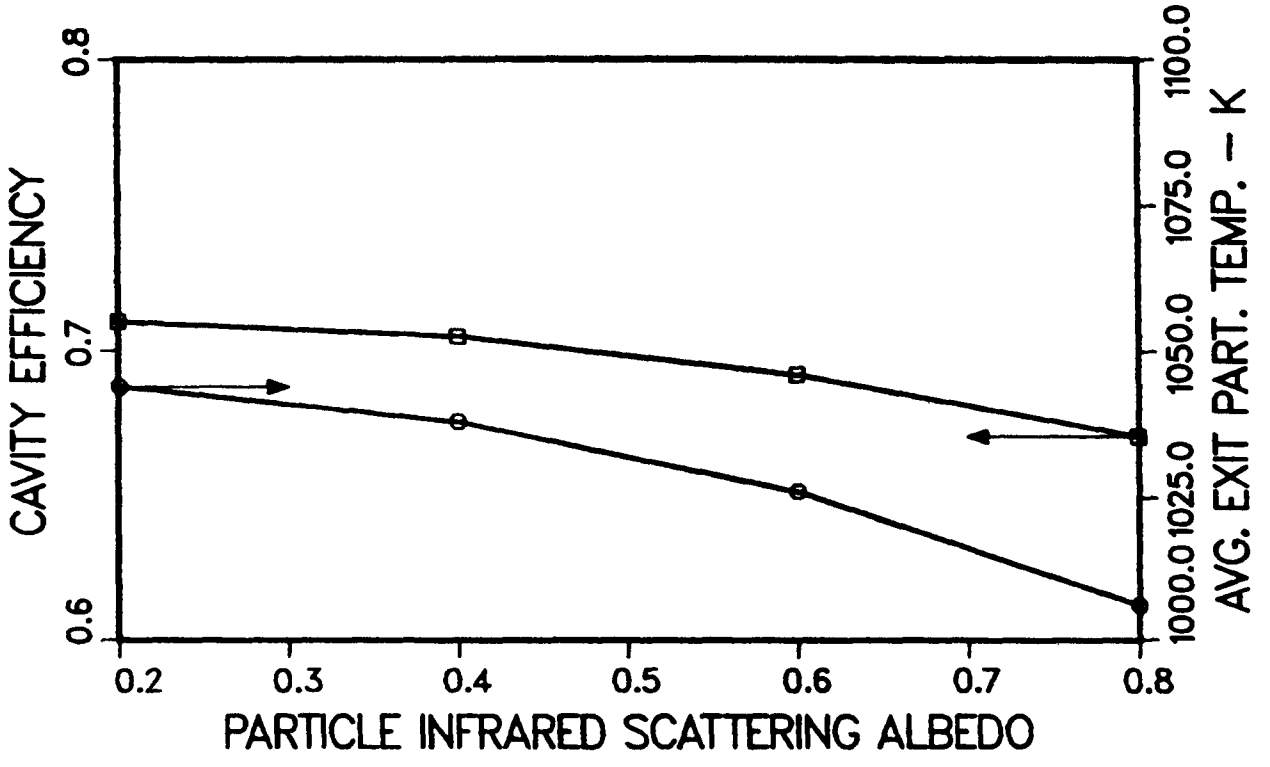

Figure 12. Variation of cavity efficiency and average exit temperature of particles as a function of the particle infrared scattering albedo.

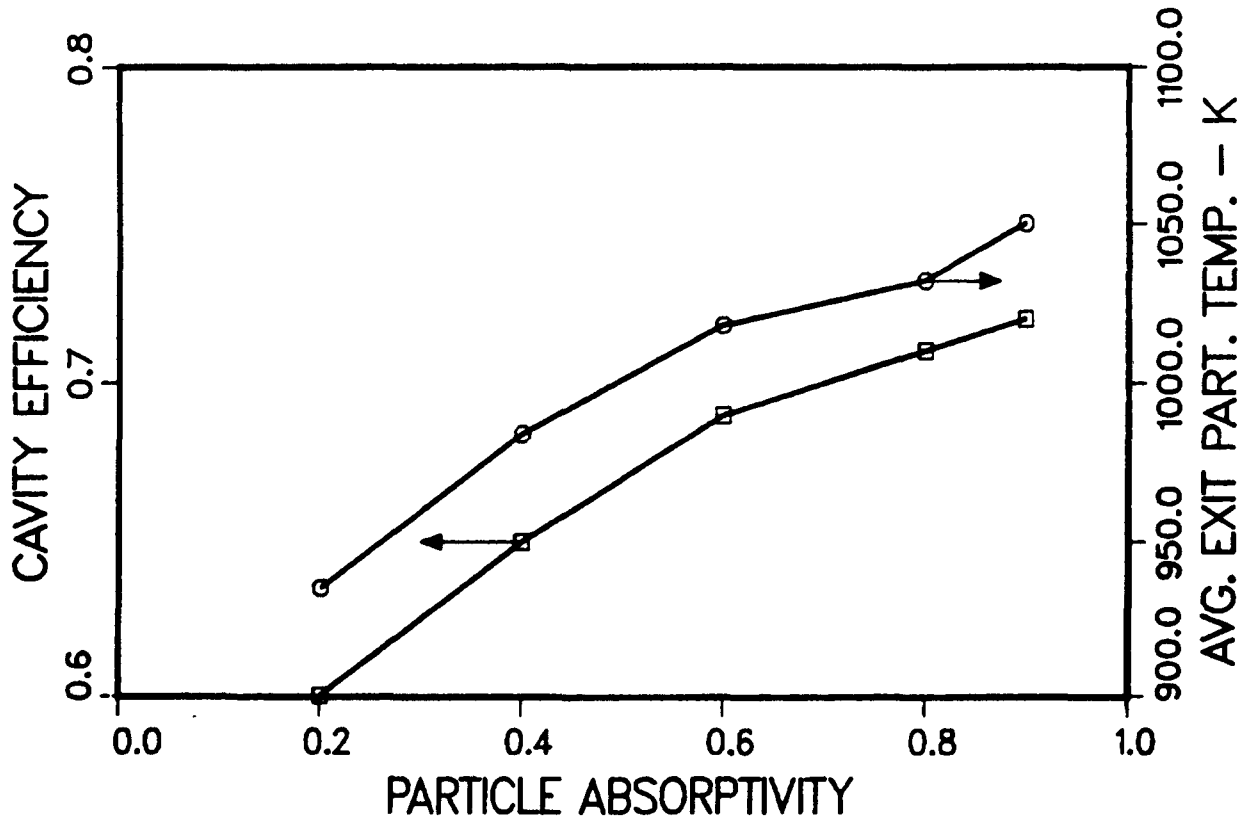

Figure 13. Variation of cavity efficiency and average exit temperature of particles as a function of the absorptivity of the particles.

of reflectivity.

Effect of Varying Receiver Geometry

The thermal performance of this two dimensional model of a solid particle receiver as a function of the size of the heliostat field was investigated for field sizes of 10^4 m^2 and 10^5 m^2. Table 1 is a listing of receiver and aperture dimensions along with total incident energy and average flux level for the two field sizes. Baseline values of aperture and receiver size and incident energy were obtained from the report of DeLaquil and Anderson (1984). In the present work, all incident energy passing through the aperture of the receiver was assumed to be incident on the particle cloud. An effective width of the particle cloud was determined based on the receiver depth and an included angle that varied between 120° and 140°, as discussed in DeLaquil and Anderson (1984). This effective width of the particle cloud was used to determine the average flux of Table 1 and to convert the total mass flow rate of the particles, described below, to units of kg/(s - meter width of particle cloud). Variations of aperture and receiver size which might be achieved by the use of a terminal concentrator (a refocusing device situated near the receiver itself) are also listed in Table 1. Calculated results of cavity efficiency, average exit temperature of the particles, and distribution of the thermal losses, for the cases of Table 1, are given in Table 2. For all cases, the average flux level was applied uniformly at the front edge of the particle cloud over the entire fall height within the receiver. The particle mass flow rate for each case was chosen to yield a nominal receiver efficiency of 70 percent and a nominal temperature rise of the particles of 800 K:

$$\dot{m} = \frac{0.7(\text{incident energy})}{800 c_{p_{part}}} \tag{25}$$

The radiative loss fraction is defined as the ratio of the amount of radiant energy leaving the cavity to the incident solar energy. According to De Laquil and Anderson (1984), approximately 11 to 12 percent of the incident energy listed in Table 1 would be lost due to spillage. The highest calculated receiver efficiency was 86 percent and was for a case representing the effects of adding a terminal concentrator to a receiver designed for a 10^5 m^2 heliostat field. For this case, the receiver dimensions were reduced by a factor of 30 percent, resulting in a higher average solar flux incident on the particle cloud. In general, higher incident solar fluxes and smaller receiver dimensions result in higher efficiencies and higher particle temperatures. As the receiver size decreases, the convective loss fraction decreases. An exception to this observation occurs for the last case of Table 2. In that case, the particle mass flow rate was significantly higher than other cases of Table 2, due to the shallower receiver, and significant air entrainment was noted for this case. In all cases, the convective heat transfer is primarily from the particles, with the walls contributing a smaller amount. Another conclusion which can be drawn from the results in Table 2 is that the radiative loss fraction decreases as the ratio of interior receiver perimeter (twice the sum of the receiver height and depth minus the aperture height) to aperture height increases, with the exception being the last case of Table 2. This last case has the smallest radiative loss fraction due to the large mass flow rate of particles and the

Table 1. Cavity dimensions and incident power levels for two heliostat field sizes.

Field Size (m^2)	Aperture Size, W x H (m x m)	Receiver Depth (m)	Receiver Height (m)	Incident Energy (MW)	Average Flux (MW/m^2)
10^{4*}	3.0 x 2.6	1.6	2.6	7.7	0.79
10^4	2.1 x 1.8	1.6	1.8	7.7	1.28
10^{5*}	7.0 x 5.8	5.0	9.5	75.0	0.65
10^5	5.0 x 4.1	5.0	9.5	75.0	0.65
10^5	5.0 x 4.1	5.0	6.7	75.0	0.92
10^5	5.0 x 4.1	3.5	6.7	75.0	1.53

* Base case receiver from DeLaquil and Anderson (1984)

Table 2. Cavity efficiency, average exit temperature of particles, and distribution of heat losses as a function of heliostat field size and cavity size.

Field Size (m^2)	Average Flux (MW/m^2)	η	$T_{p\text{exit}}$ (K)	$\frac{Q_{\text{rad loss}}}{Q_{\text{inc}}}$	$\frac{Q_{\text{cnv loss}}}{Q_{\text{inc}}}$
10^{4*}	0.79	0.59	930	0.29	0.11
10^4	1.28	0.70	1032	0.22	0.08
10^{5*}	0.65	0.59	932	0.11	0.28
10^5	0.65	0.64	973	0.09	0.26
10^5	0.92	0.70	1032	0.10	0.19
10^5	1.53	0.86	1175	0.07	0.07

* Base case receiver from DeLaquil and Anderson (1984)

increased absorption of radiation in the falling cloud.

The effect of the distribution of the incident solar flux on the efficiency of the receiver and on the temperature of the particles was examined. The results from a uniform solar flux distribution were compared with those obtained from applying the same total incident power in a variable distribution consisting of a linear variation of the solar flux over the top and bottom quarters of the cavity with a constant flux applied over the central half of the cavity. Both cavity efficiency and average exit temperature of the particles increased slightly (2 percent and 30 K, respectively) for the variable flux distribution.

Receiver Modifications for Reducing Convective Losses

The efficiency of the cavity and the temperature of the particles could be increased if the hot, buoyant air generated within the cavity due to convection from the particles and cavity walls was used to preheat the particles or was contained within the cavity. Calculations were made with different values of the back pressure parameter, K, to obtain different pressure drops at the top outlet opening. Values of K less than one would occur if a heat exchanger to preheat the particles or any other device causing a restriction to the outflow of air, such as a hopper of particles, was situated over the inlet region. At the same time a forced flow outside the cavity aperture was permitted to simulate an air window across the open cavity aperture. Figures 14a and 14b show the resulting air flow field and temperature field, respectively, which occur when a back pressure parameter, $K = 0.75$, is applied at the top outlet of the cavity, and a forced flow with free stream velocity of 3.0 m/s is directed vertically upward outside the cavity aperture. Another method of controlling convective air currents would be to replace the open aperture with a solid window transparent to solar radiation. Figures 15a and 15b show the air flow field and the temperature field, respectively, which result when a solid window that is transparent to radiation at all wavelengths is used in place of the open aperture. Table 3 contains the results for cavity efficiency, convective loss fraction, radiative loss fraction and average exit particle temperature which are obtained by varying the back pressure parameter and forced flow velocity. The results obtained using a transparent window are also shown in this table. A small convective loss occurs for the transparent window case due to the presence of an opening in the top of the cavity.

The efficiency and particle temperature do increase by applying the above modifications to the cavity design in order to reduce the convection loss. However, a cavity efficiency of about 80 percent seems to be reached for the cavity design under consideration. This is due to increasing thermal radiation losses as higher particle and cavity wall temperatures are attained. Heat losses from the receiver by conduction through the walls are omitted from Table 3; conduction through the cavity walls is estimated to be approximately one percent of the incident solar energy. The fourth entry in Table 3 has losses which are greater than $(1-\eta)$. This difference results from inaccuracies due to the combined effects of the necessarily limited resolution provided by the numerical grid and the iterative nature of the solution.

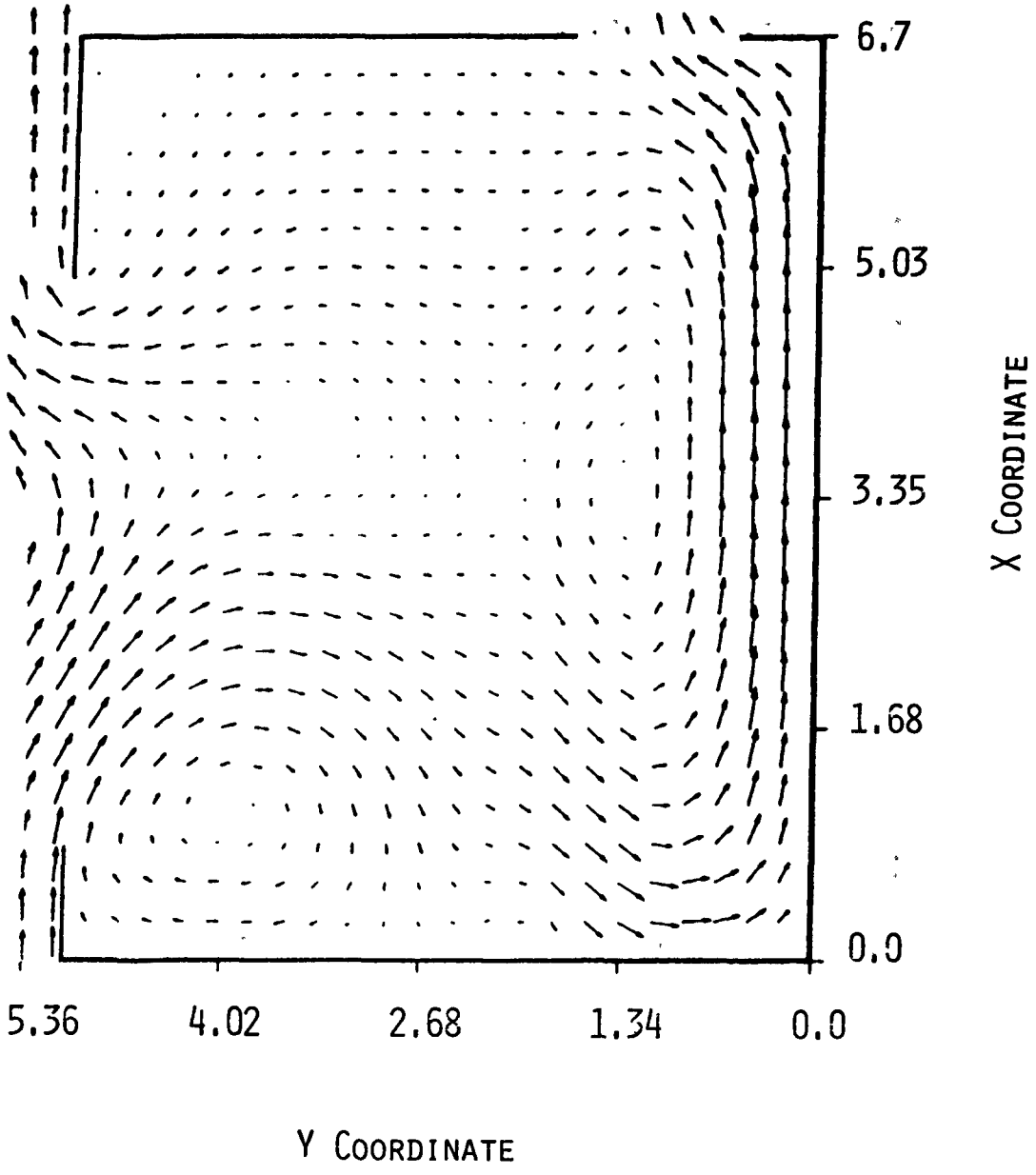

Figure 14a. Air flow field with particles with a forced flow velocity of 3 m/s applied in the positive x direction outside the cavity and the back pressure parameter, K, set to 0.75 at the top opening. The maximum air velocity in the cavity is 6 m/s.

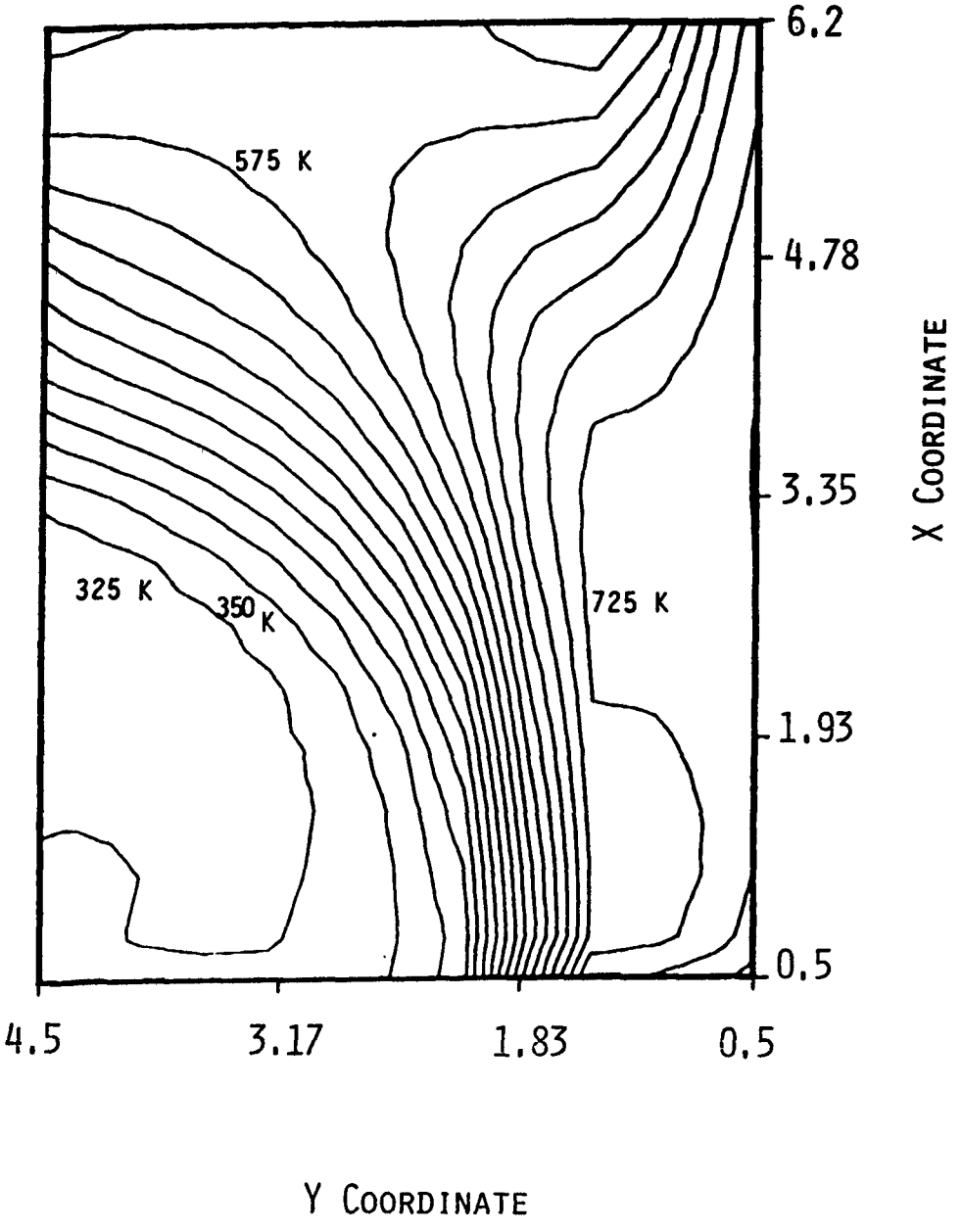

Figure 14b. Air isotherms with particles with a forced flow velocity of 3 m/s and back pressure parameter, K, set to 0.75.

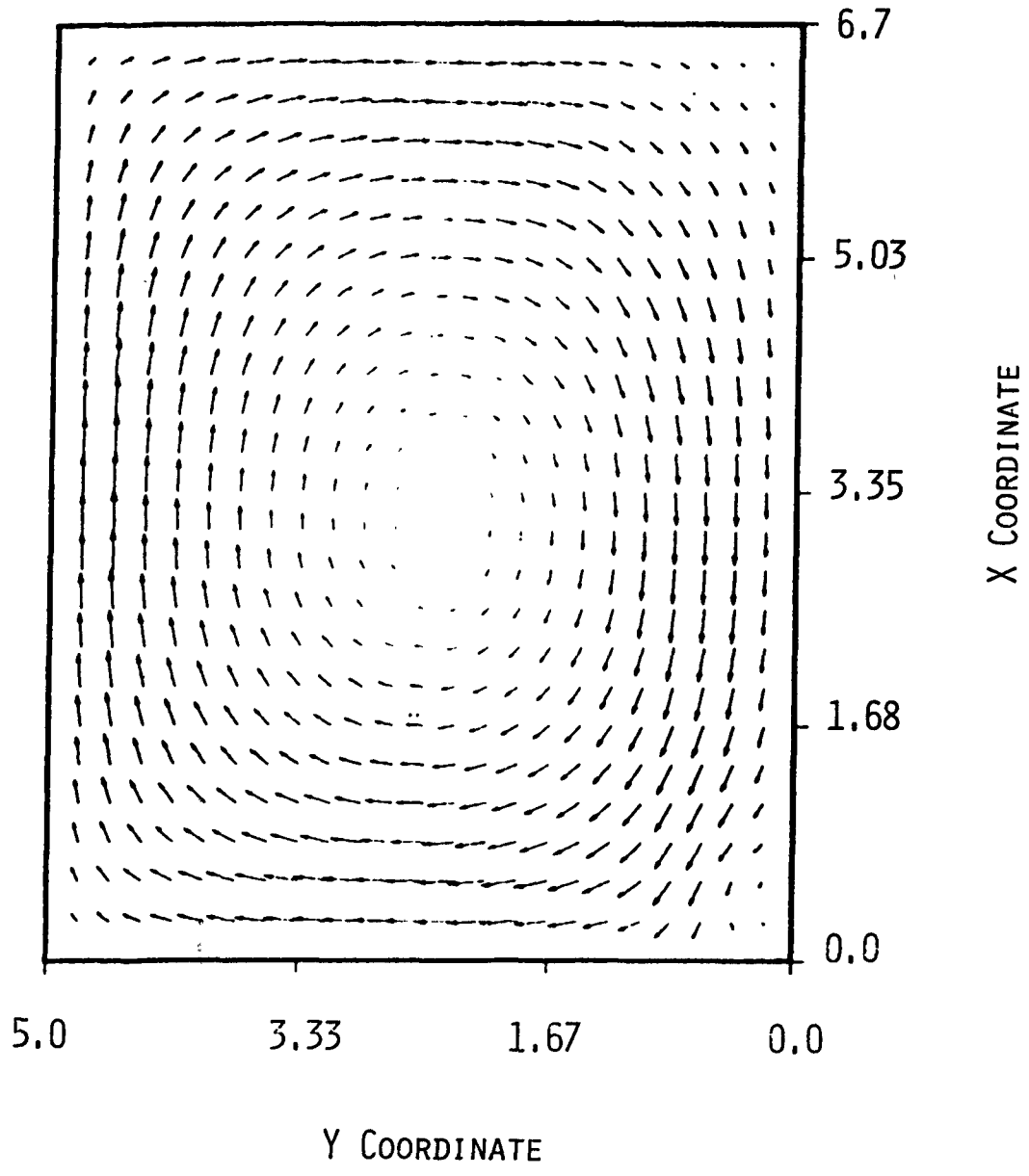

Figure 15a. Air flow field with particles with a transparent window across the aperture of the cavity. An opening is permitted at the top of the cavity. The maximum air velocity in the cavity is 6 m/s.

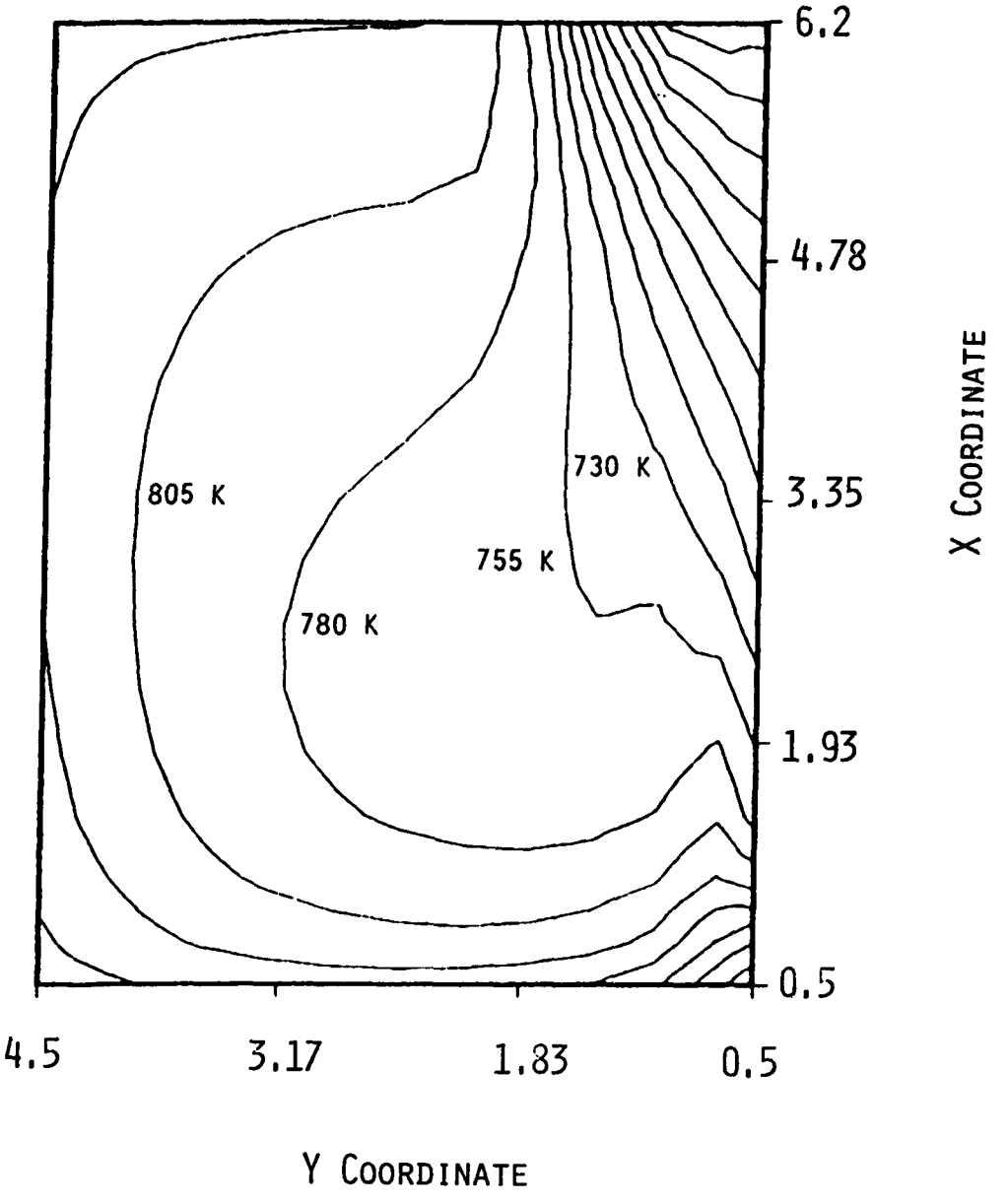

Figure 15b. Air isotherms with particles with a transparent window across the aperture of the cavity.

Table 3. Cavity efficiency, average exit temperature of particles, and heat losses by convection and radiation for various modifications to the baseline cavity (SPR base).

	SPR base $K = 1.0$	Air Window 3 m/s $K = 1.0$	Air Window 3 m/s $K = 0.75$	Air Window 3 m/s closed top	Trans. Window open top
η	0.71	0.74	0.76	0.80	0.81
$T_{p_{\text{exit}}}$	1032 K	1059 K	1089 K	1118 K	1131 K
$\frac{Q_{\text{cnv loss}}}{Q_{\text{inc}}}$	0.19	0.15	0.12	0.10	0.04
$\frac{Q_{\text{rad loss}}}{Q_{\text{inc}}}$	0.09	0.10	0.11	0.11	0.13

V. COMPARISON WITH EXPERIMENTAL RESULTS

Comparison with the Radiant Heat Facility Test

An experiment was performed at the radiant heat facility at Sandia, Albuquerque, by Hruby et al. (1984) in which the temperature and velocity of irradiated, falling clouds of particles were measured. The geometry for the experiment was limited due to the nature of the radiant heat source to a channel 10 meters high, 0.3 m wide, and 0.15 m deep. The radiation source consisted of banks of tungsten filament infrared lamps, arranged to provide a uniform heat source over the 10 meter fall height of the particles. Fused silica plates formed the front wall of the channel and separated the lamps from the particles. Radiant flux measurements were made using circular foil heat flux gauges. The particles were dropped from a hopper located just above the top of the channel. An LDV system was used to measure particle velocity. Particle temperature was measured using an insulated cup which contained a thermocouple.

Calculations were made assuming that dependent variables and properties did not vary over the width of the channel. A uniform mesh with $\Delta x = 0.55$ m in the vertical direction and $\Delta y = 0.01$ m in the horizontal direction was used. The front wall of the channel was assumed to be semi-transparent, whereas the back wall was opaque with a reflectivity of 0.5. Radiative properties of the walls and the particles were assumed to be independent of wavelength. Calculations were made using the properties of silicon carbide particles with a particle diameter of 650 microns. The single scattering albedo of the particles was assumed to be 0.2. The intensity of the radiation incident upon the semi-transparent front wall of the channel was chosen so that the calculated irradiation at the back wall of the channel matched the value measured in the experiment. Comparisons of channel efficiency (defined in the same manner as for the cavity) and average exit temperature of the particles are made for run number 502 (Hruby et al., 1984) and are shown in Table 4. Efficiency of the channel is low due to the large area of the semi-transparent front wall relative to the area of the interior walls. The various model entries in Table 4 correspond to different conditions for the transmissivity of the front wall of the channel and for the back pressure imposed at the top of the channel. The back pressure parameter, K, was varied because this has a significant effect on the air velocities in the channel and these velocities were not measured. The calculated efficiency of the cavity and the average exit temperature of the particles, however, are fairly insensitive to both the back pressure parameter and the transmissivity of the front wall. The average exit temperature of the particles was calculated at the bottom of the 10 meter channel whereas the particle temperature was measured in a catch bin below the exit of the channel. Thus, the measured particle temperature of 1125 K would be expected to be lower than the calculated values. Profiles of particle temperature shown in Figure 16 indicate that calculated temperatures (for the model with $\tau = 0.8$) exceed measured values by as much as 50-200 K inside the channel. The measured particle temperatures shown in Figure 16 have been averaged over several experiments and the

Table 4. Efficiency of energy absorption and average exit temperature of particles. Comparison of calculations and measurements for the channel geometry of the radiant heat test.

	radiant heat experiment no. 502*	model $\tau = 0.8$ $K = 0.7$	model $\tau = 0.4$ $K = 0.7$	model $\tau = 0.4$ $K = 0.65$	model $\tau = 0.1$ $K = 0.65$
η	0.116	0.117	0.122	0.125	0.126
$T_{p_{\text{exit}}}$	1125 K (in catch bin)	1117 K	1183 K	1200 K	1204 K

* Hruby et al. (1984)

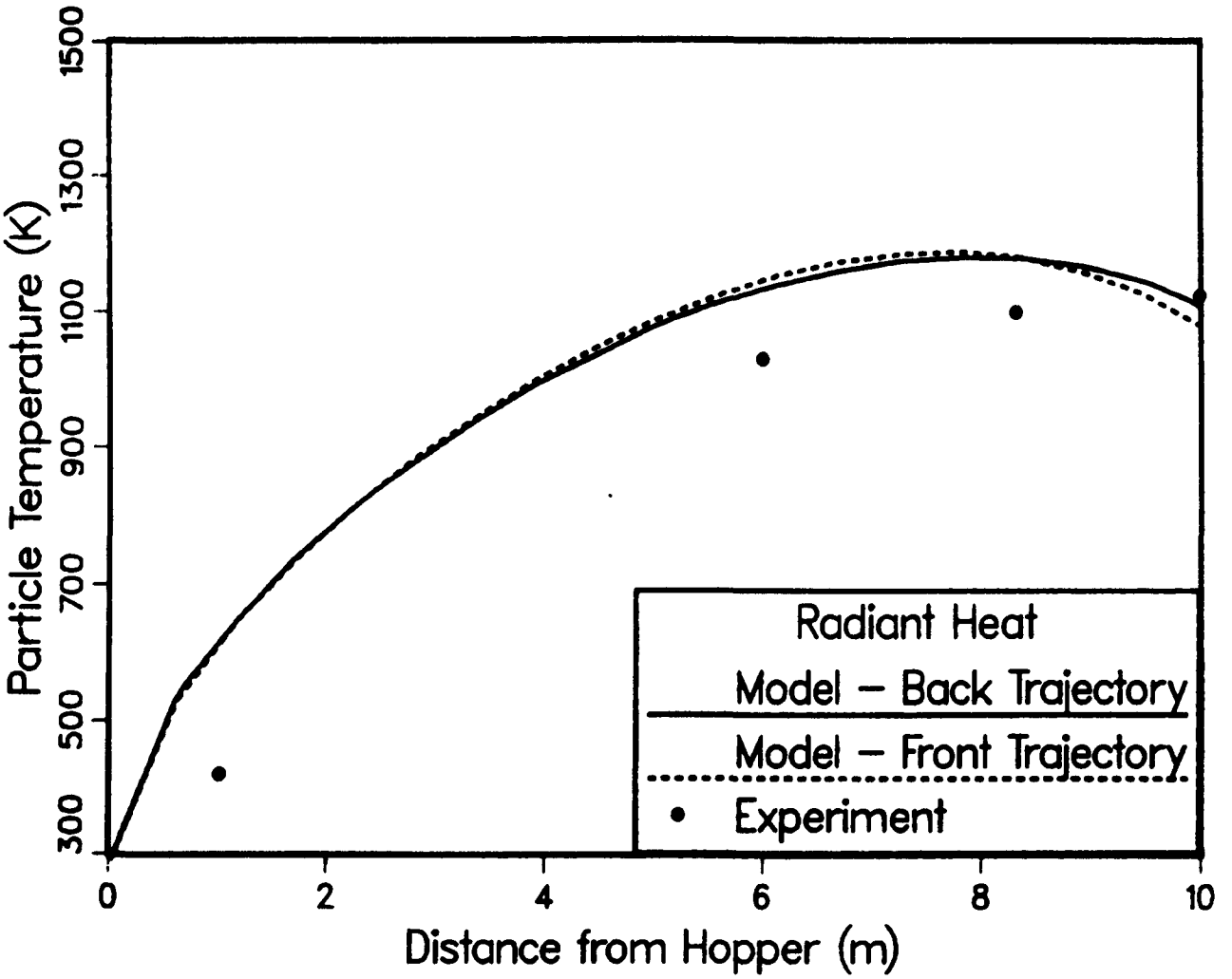

Figure 16. Calculated and measured particle temperature for the channel geometry of the radiant heat test as a function of distance from the hopper.

uncertainty in these measurements was not quantified.

Figure 17 shows the calculated (for the model with $\tau = 0.8$) and the measured vertical velocity of the particles as a function of distance from the top of the channel. The agreement is quite good for a fall distance less than 4 meters. Beyond this distance, the calculated values change very slightly while the measured value decreases by a factor of two. From the measured velocity profile, Hruby et al. (1984) concluded that this drop in velocity was due to convective air currents generated by particle heating of the air in the lower section of the channel. They also assumed that the hot rising air transferred energy to the particles in the upper portion of the channel and hence exerted less drag force on the particles in this region. The calculated profiles of air velocity and temperature show this to be the case; in fact, for most of the cases in Table 4, there is a net convective heat transfer from the air to the particles, with convective heat transfer from the walls to the air supplying the necessary energy for the air to maintain an upward movement in the channel. Calculations yield vertical air velocities $\approx$ 1.5 m/s in the lower half of the channel. Vertical air velocities decrease with height in the channel and are 50 percent lower near the top outlet of the channel. Similarly, the temperature of the air midway between the channel walls is 1200 K in the lower half of the channel, whereas the temperature of the air leaving the channel is 600 K. The calculated air velocities, however, are not large enough to cause the reduction in particle velocity that is measured. Air velocities of 4-5 m/s would be required to achieve the measured reduction in vertical velocity of the particles.

Comparison with Cold Flow Drop Tests

As previously discussed, measurements of particle velocity in falling clouds of particles indicated a significant reduction in drag from what would be experienced by a single particle in free fall (Hruby and Burolla, 1984). Initial attempts to model this gas-particle flow as a one dimensional two-phase flow were unsuccessful in predicting the fall velocity of the particles, and the reason was attributed to two dimensional effects. Using the PSI-Cell code, Crowe (1984) predicted air and particle velocities in a two dimensional, axisymmetric gas-particle flow. Measurements of particle velocity (Steeper, 1985) using LDV in a falling cloud of particles are compared in Figure 18 with calculations obtained using the PSI-Cell code. The calculations shown in this figure are for particles with a diameter of 650 microns and a material density of 3130 kg/m^3. The predictions of particle velocity using the PSI-Cell model are spread over a band, where the upper limit of particle velocity represents a particle located near the center of the cloud and the lower limit represents a particle near the outer edge of the cloud. The agreement between measurements and calculations is reasonably good, although the prediction of particle velocity gives slightly larger values at greater distances from the hopper. The particles used in the experiment have a nominal size of 650 microns with a size distribution that is unknown. The sensitivity of the calculations to particle size was examined, and the vertical velocity of 550 micron particles at a distance of 3 meters from the hopper was found to vary from 5.8 m/s at the center of the cloud to 5.3 m/s at the edge of the cloud. The calculated diameter of the particle cloud was approximately 20 cm at a distance of 3 meters from the hopper. Error bars for the experimental data are not shown on Figure 18 but an uncertainty in vertical velocity of $\pm$ 0.3 m/s for the larger velocities has been estimated by Steeper

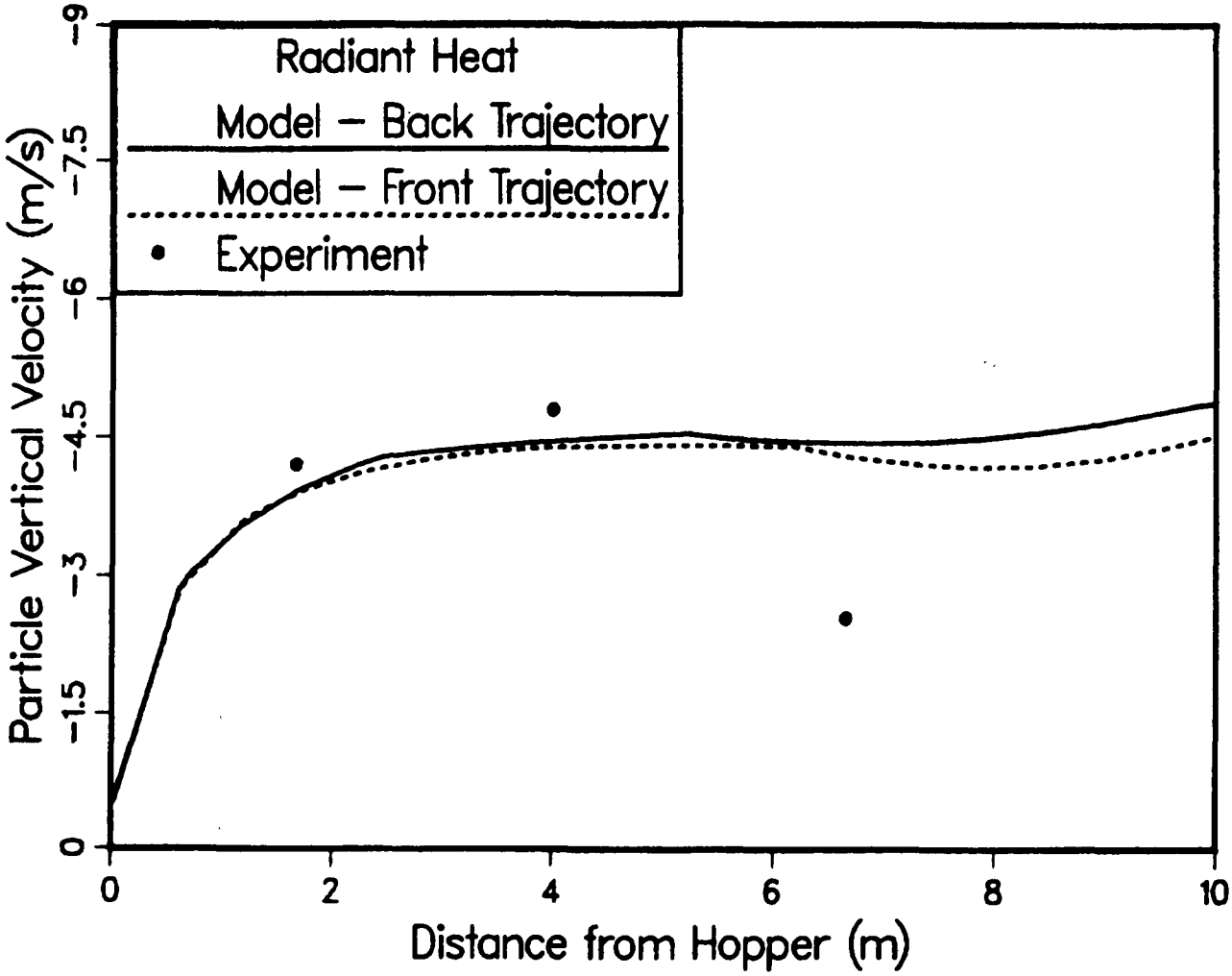

Figure 17. Calculated and measured particle vertical velocity for the channel geometry of the radiant heat test as a function of distance from the hopper.

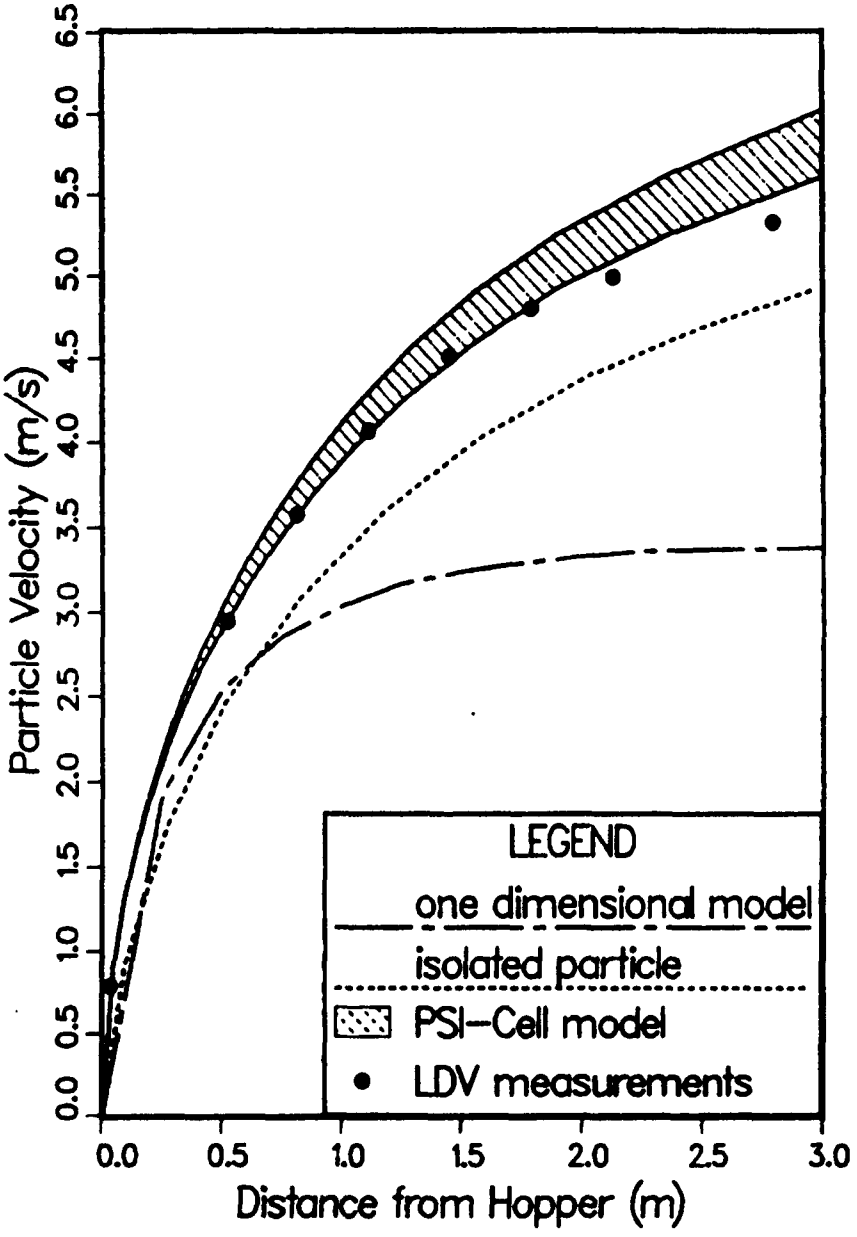

Figure 18. Calculations using various models and measurements of particle vertical velocity for a cloud of unheated Norton Co. Masterbeads falling in an isothermal, quiescent environment.

(1985). Calculations of particle velocity obtained using both a one dimensional two-phase flow model (Hruby and Falcone, 1985) and the standard isolated sphere model (with drag coefficient given by equation (14)) are also shown in Figure 18. These calculations were made for a particle diameter of 650 microns.

Profiles of particle temperature and velocity obtained from the model and the experimental determination of these quantities show similar trends for the radiant heat test. Although discrepancies exist, it is unclear whether these discrepancies are due to model deficiencies, uncertainty in boundary conditions, or uncertainty in experimental measurements. Agreement between the measured and predicted particle velocities in cold flow drop tests is reasonably good. The momentum coupling that occurs when a cloud of particles is dropped from a hopper into quiescent air is predicted by the model.

SUMMARY

A study has been made of the gas-particle flow and heat transfer in a steady, two dimensional, solid particle solar central receiver. The elliptic equations for conservation of mass, momentum, and energy of air are solved, allowing for the temperature dependence of the physical properties. The PSI-Cell model provides a Lagrangian description of the particle flow and allows for two-way coupling of momentum and heat transfer between the particles and the air. Radiation transport within the particle cloud is determined by solving the radiative transport equation on a monochromatic basis, including the effects of anisotropic scattering. Radiation transport with the cavity walls and the front surface of the particle cloud is also included. A parameter study has resulted in the following conclusions.

1. Increases in cavity efficiency are accompanied by lower particle temperatures when mass flow rate is increased.

2. Smaller particles (in conjunction with a fixed mass flow rate) result in larger optical depths, longer residence times, and higher convective losses.

3. Larger infrared scattering albedo (reduced particle emission) results in lower particle temperatures and lower cavity efficiencies. This is due to reduced absorption of the infrared radiation from the high temperature walls.

4. Convective losses from the particles represent a significant fraction of the incident solar energy unless techniques for controlling these losses, such as air windows (or transparent windows) are used.

5. Optical thickness (horizontally into the particle cloud) varies by almost an order of magnitude from the top to the bottom of the cavity due to dilution resulting from particle acceleration in the vertical direction. This effect is minimized for smaller receivers.

6. Parameter studies have shown that larger incident solar fluxes coupled with smaller receivers result in improved receiver efficiency and higher particle temperature.

NOMENCLATURE

C_D = drag coefficient

F = total radiative heat flux, W/m^2

F_λ = spectral radiative heat flux, $W/(m^2$ - micron)

$F_{\lambda,\text{for}}$ = forward spectral radiative heat flux, $W/(m^2$ - micron)

$F_{\lambda,\text{bac}}$ = backward spectral radiative heat flux, $W/(m^2$ - micron)

$F_p{}^x$ = drag force exerted on a single particle, N

I_λ = monochromatic radiative intensity, $W/(m^2$ - micron - sr)

$I_{b,\lambda}$ = Planck's function, $W/(m^2$ - micron - sr)

K = back pressure parameter

L = vertical distance from top of cavity to bottom of cavity aperture, m

$\dot{N}$ = particle number flow rate

Nu = Nusselt number = hd_p/k

P = pressure, N/m^2

P_k = Legendre polynomial of order k

Pr = Prandtl number

Q_p = heat transfer from a particle to air, W

Q_{rad} = radiation source term in particle energy equation, W

Re = particle Reynolds number $= \rho d_p \left|\vec{u}_p - \vec{u}\right| / \mu$

$S_p{}^{x,y}$ = gas x, y momentum equation source term due to particles, N

$S_p{}^T$ = gas energy equation source term due to particles, kg K/s

T = temperature, K

c_p = specific heat of air, J/(kg - K)

$c_{p_{part}}$ = specific heat of particle, J/(kg - K)

d = thickness of particle cloud, m

d_p = particle diameter, m or microns

g = acceleration due to gravity, m/s^2
= asymmetry factor for the phase function

h = heat transfer coefficient, $W/(m^2 - K)$

k = thermal conductivity, $W/(m - K)$

$\dot{m}$ = particle mass flow rate, kg/s

n = particle number density, particles/m^3

p_λ = phase function

t = time, s

Δt_i = particle transit time across a computational cell along the i^{th} trajectory, s

u = vertical velocity, m/s

v = horizontal velocity, m/s

x = vertical position coordinate, m

y = horizontal position coordinate, m

y' = horizontal position coordinate into the particle cloud, m

y^+ = dimensionless distance from a wall = $y\sqrt{\tau_w \rho/\mu^2}$ where τ_w is the wall shear stress

Δx = vertical grid spacing, m

Δy = horizontal grid spacing, m

β_λ = extinction coefficient, m^{-1}

ϵ = turbulent dissipation, m^2/s^3

θ, θ' = polar angle of coordinate system

ϕ, ϕ' = azimuthal angle of coordinate system

ξ = relative scattering angle

κ = turbulent kinetic energy, m^2/s^2

κ_λ = absorption coefficient, m^{-1}

σ_λ = scattering coefficient, m^{-1}

ρ = density, kg/m^3

λ = ratio of $C_D/C_{D_{\text{Stokes}}}$

μ = viscosity, kg/(m - s)

τ_λ = optical depth

$\tau_{\lambda,d}$ = total optical thickness of particle cloud

Ω = solid angle, sr

REFERENCES

Abdelmeguid, A. M., and Spalding, D. B., 1979, "Turbulent flow and heat transfer in pipes with buoyancy effects," J. Fluid Mech., Vol. 94, part 2, pp. 383-400.

Alpert, R. L., 1984, "Calculated Interaction of Sprays with Large-Scale Buoyant Flows," ASME, Journal of Heat Transfer, Vol. 106, pp. 310-317.

Bird, R. B., Stewart, W. E., and Lightfoot, E. N., 1960, Transport Phenomena, Wiley, p. 409.

Chen, P. P., and Crowe, C. T., 1984, "On the Monte Carlo method for modeling Particle Dispersion in Turbulence," Gas-Solid Flows, ASME Fluids Eng. Div., FED-Vol. 10, pp. 37-41.

Crowe, C. T., and Pratt, D. T., 1974, "Analysis of the Flow Field in Cyclone Separators," Computers and Fluids, Vol. 2, pp. 249-260.

Crowe, C. T., Sharma, M. P., and Stock, D. E., 1977, "The Particle-Source-in Cell (PSI-CELL) Model for Gas-Droplet Flows," ASME, Journal of Fluids Eng., pp. 325-332.

Crowe, C. T., 1980, "Modeling Spray-Air Contact in Spray-Drying Systems," Advances in Spray Drying, Hemisphere Publishing, ch. 3, pp. 63-99.

Crowe, C. T., 1984, "Results of Two-Dimensional Gas-Particle Flow Calculations Applied to the Particle Free-Fall Experiments," SNLL memo, Div. 8244, Aug. 15.

De Laquil III, P., and Anderson, J. V., 1984, "The Performance of High- Temperature Central Receiver Systems," Sandia National Laboratories, SAND84-8233.

El-Bainhawy, V., and Whitelaw, J. H., 1980, "The Calculation of the Flow Properties of a Confined Kerosine-Spray Flame," AIAA Journal,Vol. 18, no. 12, pp. 1503-1510.

Eschbach, E. J., and Stock, D. E., 1979, "Optimization of Collection Efficiency by Varying Plate Spacing with an Electrostatic Precipitator," Proceedings of the 2nd EPA Conference on Transfer and Utilization of Particulate Control Technology, Denver.

Falcone, P. K., Noring, J. E., and Hackett, C. E., 1982, "Evaluation and Application of Solid Thermal Energy Carriers in a High Temperature Solar Central Receiver System," presented at 17th IECEC, Los Angeles.

Gosman, A. D., and Pun, W. M., 1973, "Calculation of Recirculating Flow," Lecture

Notes, Imperial College of Science and Technology, London, England.

Houf, W. G. and Greif, R., 1985, "Radiation Transfer in a Solar Absorbing Particle Laden Flow," Radiation Heat Transfer, ASME HTD- Vol. 43, eds. Armaly, B. F., and Emery, A. F., pp. 9-14.

Hruby, J. M. and Burolla, V. P., 1984, "Solid Particle Receiver Experiments: Velocity Measurements," Sandia National Laboratories, SAND84-8238.

Hruby, J. M., Steele, B. R., and Burolla, V. P., 1984, "Solid Particle Receiver Experiments: Radiant Heat Test," Sandia National Laboratories, SAND84-8251.

Hruby, J. M., and Falcone, P. K., 1985, "Momentum and Energy Exchange in a Solid Particle Solar Central Receiver," Heat Transfer - Denver 1985, AIChE Symposium Series, N. M. Farukhi, ed., Vol. 81, no. 245, pp. 197-203.

Humphrey, J. A. C., Sherman, F. S., and To, W. M., 1985, "Numerical Simulation of Buoyant Turbulent Flow," Sandia National Laboratories Contractor Report: SAND85-8180, UC-62.

Jones, W. P. and Launder, B. E., 1972, "The prediction of laminarization with a 2-equation model of turbulence," Int. J. Heat Mass Transfer, Vol. 15, pp. 301-314.

Launder, B. E., 1984, "Numerical computation of convective heat transfer in complex turbulent flows: time to abandon wall functions?," Int. J. Heat Mass Transfer, Vol. 27, no. 9, pp. 1485-1491.

Launder, B. E., and Spalding, D. B., 1972, Mathematical Models of Turbulence, Academic Press.

Martin, J. and Vitko, J., 1982, "ASCUAS: A Solar Central Receiver Utilizing a Solid Thermal Carrier," Sandia National Laboratories, SAND82-8203.

Mason, H. B. and Seban, R. A., 1974, "Numerical Predictions for Turbulent Free Convection from Vertical Surfaces," Int. J. Heat Mass Transfer, Vol. 17, pp. 1329-1336.

Patankar, S. V., 1980, Numerical Heat Transfer and Fluid Flow, McGraw-Hill.

Plumb, O. A. and Kennedy, L. A., 1977, "Application of a κ- ϵ Turbulence Model to Natural Convection From a Vertical Isothermal Surface," ASME, Journal of Heat Transfer, Vol. 99, no. 1, pp. 79-85.

Rudinger, G., 1980, "Fundamentals of Gas-Particle Flow," Handbook of Powder Technology, Vol. 2, p. 105, Elsevier.

Siegel, R. and Howell, J. R., 1981, Thermal Radiation Heat Transfer, 2nd ed., McGraw-Hill.

ω_λ = single scattering albedo

subscripts

b = blackbody

eff = effective viscosity or conductivity

i = for the i^{th} trajectory

p = particle phase

turb = turbulent quantity

λ = wavelength dependence

∞ = evaluated at ambient conditions

superscripts

i = initial particle conditions

Soo, S. L., 1967, Fluid Dynamics of Multiphase Systems, p. 73, Blaisdell Publishing Co.

Spalding, D. B., 1972, "A Novel Finite-Difference Formulation for Differential Expressions Involving Both First and Second Derivatives," Int. J. Num. Methods Eng., Vol. 4, pp. 551-559.

Stahl, K. A., Griffin, J. W., and Pettit, R. B., 1985, "Optical properties of solid particle receiver materials II: diffuse reflectance of Norton Masterbeads at elevated temperatures," SPIE Optical Materials Technology for Energy Efficiency and Solar Energy Conversion, no. 4, paper no. 562-30, San Diego.

Steeper, R., 1985, private communication.

Wallis, G. B., 1969, One-Dimensional Two-Phase Flow, McGraw-Hill.

White, F. M., 1974, Viscous Fluid Flow, McGraw-Hill.

UNLIMITED RELEASE
INITIAL DISTRIBUTION

U.S. Department of Energy (6)
Code CE-314
Forrestal Building
1000 Independence Avenue, S.W.
Washington, D.C. 20585
Attn: H. Coleman
S. Gronich
C. Mangold
F. Morse
M. Scheve
R. Shivers

U.S. Department of Energy
Code CE-33
Forrestal Building, Rm. 5H095
1000 Independence Avenue, S.W.
Washington, D.C. 20585
Attn: C. Carwile

U.S. Department of Energy (2)
1333 Broadway
Oakland, CA 94612
Attn: R. W. Hughey
M. Lopez

U.S. Department of Energy
Albuquerque Operations Office
P.O. Box 5800
Albuquerque, NM 87115
Attn: J. Weisiger

North Carolina State Univ.
Chemical Engr. Dept.
P. O. Box 7905
Raleigh, NC 27695
Attn; Prof. R. Carbonell

University of California (2)
Mechanical Engineering Dept.
Berkeley, CA 94720
Attn: J.A.C. Humphrey
R. Greif

Univ. of California-Irvine
Dept. of Mech. Engineering
Irvine, CA 92717
Attn: M. Young

University of Houston
Solar Energy Laboratory
4800 Calhoun
Houston, TX 77004
Attn: A. F. Hildebrandt

University of Utah (2)
Dept. of Mechanical and
Industrial Engineering
Salt Lake City, UT 84112
Attn: M. Quinn Brewster
R. F. Boehm

Washington State University
Dept. of Mech. Engineering
Pullman, WA 99164-2920
Attn: C. T. Crowe

Arizona Public Service Co.
P.O. Box 21666
Phoenix, AZ 85035
Attn: E. Weber

Babcock and Wilcox
91 Stirling Avenue
Barberton, OH 44203
Attn: G. Grant

Battelle Pac. Northwest Labs.
P. O. Box 999
Richland, WA 99352
Attn: T. A. Williams

Bechtel Group, Inc.
(5014/C11)
P.O. Box 3965
San Francisco, CA 94119
Attn: P. DeLaquil

Black and Veatch
Consulting Engineering
P.O. Box 8405
Kansas City, MO 64114
Attn: J. C. Grosskreutz

Boeing Aerospace Company
Energy Systems
P.O. Box 3999, MS87-63
Seattle, WA 98124
Attn: W. D. Beverly

Centre National De La
Recherche Scientifique
Laboratorie d'Energetique
Solaire
Odiello, B.P. 5
66120 Font-Remeu
FRANCE
Attn: C. Royere

El Paso Electric Company
P.O. Box 982
El Paso, TX 79946
Attn: J. E. Brown

Electric Power Research Inst.
P.O. Box 10412
Palo Alto, CA 94303
Attn: E. DeMeo

Foster Wheeler Develop. Corp.
12 Peach Tree Hill Road
Livingston, NJ 07039
Attn: R. J. Zoschak

Garrett-AiResearch Mfg. Co.
2525 W. 190th St.
Torrance, CA 90509
Attn: M. Combs

G. A. Technologies
P.O. Box 85608
San Diego, CA 92138
Attn: G. Besenbruch

Georgia Institute of Tech.
Atlanta, GA 30332
Attn: R. A. Cassanova

Gibbs and Hill, Inc.
393 Seventh Avenue
New York, NY 10001
Attn: R. Prieto

IEA/SSPS Project
Apartado 649
Almeria, Spain
Attn: C. Arano

Laboratorie D'Energetique
Solaire
40 Avenue de Recteur Pineau
86022 Poitiers
FRANCE
Attn: P. LeQuere

Lawrence Berkeley Labs.
University of California
Berkeley, CA 94720
Attn: A. J. Hunt

Los Angeles Deptment
of Water and Power
111 North Hope St.
Los Angeles, CA 90051
Attn: D. Chu

McDonnell Douglas
Astronatics Co.
5301 Bolsa Avenue
Huntington Beach, CA 92647
Attn: R. L. Gervais

Olin Chemical Company
120 Long Ridge Road
Stamford, CT 06904
Attn: L. C. Fioruccio

Pacific Gas and
Electric Company (3)
3400 Crow Canyon Road
San Ramon, CA 94526
Attn: G. Braun
J. Iannucci
C. Weinburg

The Ralph M. Parsons Co.
100 West St.
Pasadena, CA 91124
Attn: N. W. Snyder

Polydyne, Inc.
1900 S. Norfolk St.
Suite 209
San Mateo, CA 94403
Attn: P. B. Bos

Resource Analysis, Inc.
P.O. Box 91890
Los Angeles, CA 90009
Attn: T. Rosenman

San Diego Gas and Electric Co.
Mechanical Engineering
P.O. Box 1831
San Diego, CA 92112
Attn: R. E. Potthoff

Solar Energy Industries
Association
1717 Massachusetts Ave., N.W.
Suite 503
Washington, D.C. 20035
Attn: C. LaPorta

Solar Energy Research Inst. (5)
1617 Cole Boulevard
Golden, CO 80401
Attn: M. Carasso
B. Gupta
D. Johnson
F. Kreith
K. Y. Wang

Solar Power Engineering Co.
P.O. Box 91
Morrison, CO 80465
Attn: H. C. Wroton

Southern California Edison
P.O. Box 800
Rosemead, CA 82807
Attn: J. N. Reeves

Spectra Technology, Inc.
2755 Northrup Way
Bellevue, WA 98004
Attn: R. R. Taussig

Stearns Catalytic Corp.
P.O. Box 5888
Denver, CO 80217
Attn: W. R. Lang

O. Walton, LLNL, L-200
J. W. Nunziato, 1510

D. W. Larson, 1513

E. H. Beckner, 6000
Attn: V. Dugan, 6200
J. Holmes, 6226
J. Otts, 6226

R. S. Claassen, 8000
Attn: E. E. Ives, 8100
A. N. Blackwell, 8200
D. L. Hartley, 8300

C. W. Robinson, 8240
Attn: G. A. Benedetti, 8241
M. L. Callabresi, 8242
M. R. Birnbaum, 8243
C. M. Hartwig, 8244

G. H. Evans, (20)
W. G. Houf, 8245
R. J. Kee, 8245
C. A. LaJeunesse, 8245
S. Paolucci, 8245

R. C. Wayne, 8400
Attn: L. D. Bertholf, 8430
H. Hanser, 8440

M. Abrams, 8431
R. L. Rinne, 8470
A. C. Skinrood, 8471
P. K. Falcone, 8471
J. M. Hruby, 8473 (5)
R. R. Steeper, 8473
J. C. Swearengen, 8473
M. E. John, 8478

Publications Division, 8265
for TIC (30)

Publications Division 8265/
Technical Library Processes
Division, 3141

Technical Library Processes
Division 3141 (3)

P. W. Dean, 8024, for
Central Technical Files (3)

DO NOT MICROFILM
COVER

Org.	Bldg.	Name	Rec'd by	Org.	Bldg.	Name	Rec'd by

Sandia National Laboratories